Hysteresis Behavior Patterns in Complex Systems

A Thesis

Submitted to the Faculty

of

Drexel University

by

Ondrej Hovorka

in partial fulfillment of the

requirements for the degree

of

Doctor of Philosophy

August 2007

Dedicated To

Dr. Andrej Jaroševič

Acknowledgements

First, I would like to thank my advisor, Prof. Gary Friedman, for educating me, for giving me so much freedom, for all those interesting discussions, and for being so supportive in every imaginable respect. It is hard to express how lucky I am to work with him, and generally, to know him. I would also like to express my thanks to Dr. Andreas Berger, collaboration with whom was, and continues to be, a fantastic educational experience.

I am grateful to all my PhD committee members: Prof. Adam Fontecchio, Prof. Jaudelice Cavalcante de Oliveira, Prof. Nagarajan Kandasamy, and Prof. Alexander Fridman for their encouragement and for useful suggestions to improve this thesis.

I have spent long hours discussing scientific, philosophical, and other kinds of questions with my friends Roman Gröger, Ben Yellen, Hemang Shah, Ruchita Vora, Vasileios Nasis, Greg Fridman, Kara Heinz, Halim Ayan, Eda Yildirim, Alex Chirokov, Alex Fridman, Anna Fox, Derek Halverson, Dave Delaine, Kashma Rai, Sameer Kalghatgi, William Norman, Mike Warde, Pavol Pčola, Ivan Oprenčák, and many others. Each of them played part in composing this thesis.

I want to thank my wife Veronika, for her love, for taking care of everything needed to be taken care of, for her unbelievable patience, and generally, for being my wife. Many thanks go to all my family for their support, and to my brother Michal who serves me as an example.

Table of Contents

List of Figures

Abstract

Hysteresis Behavior Patterns in Complex Systems
Ondrej Hovorka
Gary Friedman, Ph.D.

Many complex systems such as magnets, shape memory alloys, as well as socioeconomic and biological systems are known to display hysteresis. This inherently irreversible process differs from the other irreversible processes most often addressed in literature by the memory that persists long after the external parameters stop changing. In general, hysteresis is a consequence of multi-scale system dynamics and the existence of many metastable states. Although hysteresis is typically illustrated by closed minor loops, other types of hysteretic trajectories are often observed where closed loops form gradually after several external parameter periods or not at all. The question arises: What in the structure of a system determines these qualitatively different behaviors of hysteretic trajectories?

This thesis models complex hysteretic systems using a network of bistable binary elements and investigates network structure induced changes in hysteretic behavior. The main focus is on studying the minor loop formation processes for a single cyclically varying external parameter. Stable minor loops are observed to form at different rates as a function of the number of cycles, depending on the sign of the interactions, disorder level, and on the connectivity and topology of the interaction networks. For certain dense interaction networks, hysteretic trajectories that do not converge to a minor loop after an arbitrarily large number of external parameter periods are discovered. It is shown that their appearance is related to the presence of specific topological structures in the network. Thus, the thesis demonstrates several interesting links between hysteretic behavior and the underlying structure of complex systems.

Chapter 1. Scope of the thesis

This thesis describes analysis of a class of complex systems with hysteresis, which can be viewed as networks of interacting bistable elements. Typically, the term 'complex system' refers to a system consisting of many similar components, the interactions between which create behavior that cannot be associated with the individual components themselves. Such behavior is often called emergent. Several different types of emergent properties have been investigated for various types of complex systems. Among these properties are self-similarity in geometrical patterns and patterns in dynamic processes, such as power law scaling in the frequency spectrum of the system's evolution. Hysteresis is another example of emergent behavior. It can be defined as any relationship between the state of the system and external parameters, which depends on the history of the external parameter variation, but not on the rate of this variation. Hysteresis is observed in many systems such as magnets, type-II superconductors, shape memory alloys, as well as socioeconomic and biological systems. This inherently irreversible process is a consequence of existence of many metastable states and of multi-scale system dynamics.

Several interesting and widely observed features of hysteretic processes such as power laws in the avalanche statistics have been investigated before. This thesis focuses on the behavior of hysteretic processes in response to periodic variations of external conditions whenever these can be described by a single real valued variable. In part, this work is motivated by classical studies of cyclical behavior in non-linear dynamic systems where response to periodic variations of the external variables is known to be closely related to the structure of the system. Although hysteretic systems can be viewed as a particular case of non-linear dynamic systems, cyclic hysteretic processes have not been widely studied. As a result, hysteresis is typically

illustrated by closed loops in response to a periodic variation of an external parameter. However, many other types of hysteretic trajectories can be observed where closed loops form either gradually after several periods or not at all. Using a network of interacting binary elements as a model, it is shown in this thesis that behavior of hysteretic cycles is closely related to the sign of the interactions, their strength relative to an inherent fixed disorder in the system, and to the network structure.

More specifically, it will be shown that positive interactions result in the return point memory (RPM) property responsible for the recovery of system's original internal state after every external parameter period, and leading to the formation of closed minor loops at the end of the very first period. While such closed cycles are also observed for some networks with negative interactions, it generally takes several external parameter periods before a steady state with stable minor loops is reached. It will be shown that the convergence to the steady state depends significantly on the magnitude of interactions and on their topological structure. In addition, we demonstrate the possibility of behavior not observed in binary networks previously, where cycles become non-convergent and never form stable minor loops. Such non-convergent cycles are shown to be associated with specific topological elements in the network structure, suggesting that hysteretic trajectories can yield information about the inherent structure of the complex systems.

The thesis is organized as follows. In Chapter 1 we introduce basic hysteresis terminology and describe various types of hysteresis behaviors observed in systems of different nature. In Chapter 2, most widely used models of hysteresis, such as Preisach model and Random Field Ising model, are reviewed and their main properties are summarized. The notion of a random network is introduced and some elements of the graph theory are subsequently summarized. In Chapter 3 and in the following chapters, these networks are used to formulate the complex system model called Random Coercivity Interacting Switch (RCIS), which is employed as a proto-

type of hysteretic systems in the thesis. In Chapters 5-7 different interaction networks are considered and types of hysteretic cycles observed in such networks are studied. Particularly, it is shown in Chapter 5 that minor cycles are always closed if interactions are positive. Two examples of negative interaction networks which also produce only closed cycles are then discussed. These are: 1) the mean field RCIS model on a fully connected network, where every bi-stable element interacts with every other element in the network, and 2) the Néel's mean field model. In the case of the Néel's mean field model, there exists certain interaction strength where open cycles appear abruptly. In Chapter 6 we consider regular lattice networks with interaction between the immediate neighbors only. It is shown, that minor loops are formed quickly in these systems after a few external parameter periods. In Chapter 7, the interactions are modeled using random networks. It is shown that the network connectivity and topology play the key role in determining the rate of the minor loop formation. New types of cyclic trajectories are discovered, which do not form minor loops after an arbitrarily large number of external parameter periods. It is shown that they are associated with the presence of complete subgraph structures in the network. Finally, in Chapter 8, some issues related to energy loss during hysteretic processes are briefly addressed. The thesis is then concluded by summarizing the main results and discussing several future research paths with some potential applications.

Chapter 2. Introduction

Firstly, it is important to establish some terminology and a general systems background relevant to this thesis. Complex systems typically have many degrees of freedom. In magnetic systems such degrees of freedom may be associated with electronic spins. In living cells, they can be associated with concentrations of various proteins. In economic system, they correspond to different choices of every independent economic agent (firm, individual, etc). Jointly, variables that describe the system's degrees of freedom define the state of that system.

A variational principle will be used in this thesis to formulate hysteresis models. It is common to describe many systems in nature using variational principles, where the system evolves towards the state which minimizes or maximizes some state function. In economics, for example, it is the maximization of a utility function which drives the evolution of the system. In physics, energy minimization is such a variational principle. In this thesis, physical systems will be viewed as a prototype for complex systems of different natures. For this reason, terminology based on the energy minimization will be used to describe the system evolution. Moreover, among different physical systems, magnetic systems are chosen here as the primary example. For this reason, the term field (magnetic field) is often used interchangeably with the term external parameter and the term magnetization is often used to describe the average state of the system in this thesis. Similarly, the term spin is often employed to describe binary elements of the system being modeled.

It is important to realize that variational principles *do not* always have independent meaning. In many cases, they can simply be viewed as an alternative formulation of system dynamics. In classical mechanics, for example, knowledge of forces completely describes the dynamics of a system. Forces in conservative systems can be

formulated as being equal to negative gradients of the potential energy, and mechanical equilibrium where the potential energy is minimized or maximized, corresponds to the situation when net forces are zero. The potential energy minima correspond to stable equilibria because small deviations away from such equilibria generate forces that tend to bring the system back. Although systems considered in this thesis cannot be described using mechanical forces in general, the analogy that stable equilibria correspond to energy minima, and that local force driving the system is a variation of the energy function with respect to the local degree of freedom, will still be adopted here.

While some variational principles are just alternative formulations of the systems dynamics, other variational principles often *do* have independent meaning, particularly in situations where the state of the system is subject to statistical fluctuations. In physical systems, such fluctuations are due to temperature. In the presence of thermal fluctuations, the system tends towards the thermodynamic equilibrium, instead of the mechanical equilibrium, which can only be described in statistical terms. In the state of thermodynamic equilibrium a universal probability distribution, the one which maximizes the entropy for an isolated system, describes the probability that a particular microscopic state of the system is observed. The variational principle that describes the tendency of a system toward such a universal statistical description is called the second law of thermodynamics. This variational principle has not been derived from the laws of mechanics (nobody found a way to do it yet). Instead, it is independently postulated because it appears to provide a very accurate description of reality.

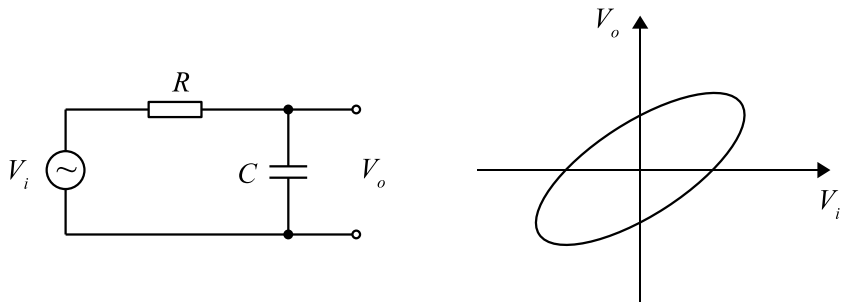

Figure 2.1: Linear RC circuit and the (non-hysteretic) dependence of the output voltage V_0 across the capacitor on the input voltage V_i. Elliptic loop is due to the phase shift between the input and output and its size and orientation depends on the frequency.

2.1 Hysteresis: History, rate independence and multiple time scales

What is hysteresis and what is not? Hysteresis can be defined simply as a relationship between the state of the system and the external parameters where the state depends on the history of the external parameters but not on their rate of variation. Dependence of the state on past values of the external parameters is not all that remarkable. Such dependences can be found even in linear systems. For example, the simple linear circuit shown in Figure 2.1 which consists of a resistor and capacitor connected in series would display dependence of the voltage across the capacitor V_0 on the past values of the voltage applied to the circuit V_i. In this case, however, the effect of the past values depends on the rate at which the voltage applied to the circuit varies. When the variation of the input voltage is sufficiently fast, a loop can be traced as illustrated in Figure 2.1. For slow variations (variations that are small during the time equal to the RC time constant), the voltage across the capacitor simply follows the applied voltage V_i and no history dependence is observed. Thus, it is the lack of dependence on the rate of the external parameter variation, as well as memory of the past values that distinguish hysteretic systems from other much simpler systems.

In what types of systems can hysteresis be observed? In the above example, the system had a single characteristic relaxation time determined by the RC constant of the circuit. More than a single characteristic time is required for a system to display hysteresis. Hysteresis is typically observed in those systems where, following a disturbance, some parts of the system re-organize well before the system as a whole reaches thermal equilibrium with its environment. In magnets, the parts of the system that re-organize quickly form magnetic domains. The time required for a domain to form or re-orient is on the order of tens of nanoseconds, while relaxation to thermal equilibrium, when all domains are oriented randomly, can take hundreds of years. Magnetic recording relies on the stability of such memory of the past state. In populations of cells, individual cells can assume some state of a protein expression quickly, well before the cellular population as a whole had a chance to randomize.

How does this separation of time scales explain emergence of hysteresis? The first part of the explanation involves introduction of an appropriate energy functional. The key point here is that, on a time scale longer than the fast re-organization time, one can treat the quickly re-organizing parts of the system as single indivisible entities, and ignore various degrees of freedom within them. This permits the redefinition of the system's degrees of freedom and drastically reduces their number. Such a process is often called coarse-graining and allows the formulation of a description of the system via an energy functional that depends only on the reduced number of the re-defined degrees of freedom. In physics, such a reduced free energy functional is often called Landau free energy.

Due to various constraints and the fixed disorder present (usually in the form of inhomogeneous properties), there are hindrances to reorganization of different parts of the system. Overcoming these hindrances requires different amounts of energy. Consequently the coarse-grained Landau free energy has a complicated structure with multiple minima separated by large barriers. When these barriers are present, the

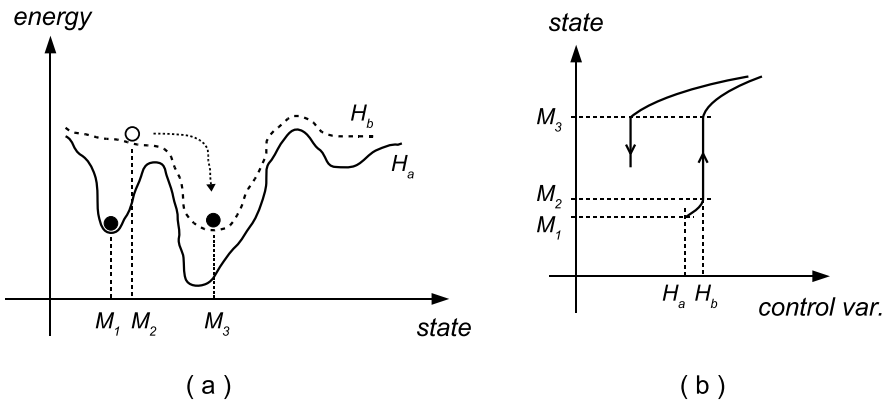

Figure 2.2: Origins of hysteresis. (a) The free energy landscape as a function of state variable M for two different values of the external parameter H. As H changes, the energy landscape becomes distorted and transitions between different states become possible. (b) Due to very short time scale, the transition between different states appears as being sharp if plotted in the state vs. external parameter plane. When the external parameter returns to the original value H_a, the state variable does not, and hysteresis is displayed.

system whose state is initially arranged to be around one of the minima will tend to linger there for a long time even in the presence of thermal fluctuations. The lingering effect is exactly what makes the re-organization time much shorter than the time of relaxation to thermal equilibrium. This would not have happened without sufficiently high free energy barriers. Thus, separation of time scales inevitably leads to the conclusion that the evolution of the system can be described by a free energy function, which can on an intermediate time scale be treated like a potential energy with multiple stable states. The system will rapidly re-arrange itself to minimize this potential energy by loosing energy quickly through transfer to hidden (due to coarse-graining) degrees of freedom.

The second part of the explanation of hysteresis involves understanding the effects of external parameters on the free energy function. As external parameters vary, the energy supplied to the system changes resulting in distortions of the energy landscape. An illustration of this is shown in Figure 2.2. Let us suppose that system originally

occupies a state near the energy minimum at the point M_1. As the external parameter varies and the energy landscape changes, the system remains in the original energy minimum as long as it exists, and any change of the state variable is reversible (Figure 2.2(a)). At some value of the external parameter (H_b), however, the original energy minimum may disappear (at M_2) and the system is forced to make a fast transition to another energy minimum corresponding to the state M_3. If after that the external parameter returns to its original value H_a, the system will still remain in this new energy minimum. Therefore, for any given value of external parameter the system may be in different states corresponding to different energy minima. The actual state assumed by the system will depend on the history of the external parameter variation.

The above discussion demonstrates how the separation of time scales, for fast reorganization of system's parts and for relaxation to thermal equilibrium, results in dependence of the state on the history of external parameter variation. What remains is to explain the rate independence. Rate independence is the result of adiabatic behavior of the system due to the separation of time scales. Adiabatic limit simply means that external parameters do not change appreciably during the fast transition from one stable state to another, and one can essentially ignore the details of how the system moves between two stable states. In fact, in many experiments, transitions between stable states can be viewed as nearly instantaneous jumps (Figure 2.2(b)). In magnetism, such jumps are often called Barkhausen jumps. In mechanics, they are called the Keiser effect. One can also hear such jumps when milk is poured into a bowl of Rice Krispies cereal as it rapidly invades the pores within the cereal grains.

In summary, hysteresis owes its existence to the separation of time scales. It can be observed only on a certain intermediate time scale, which is much longer then the fast system dynamics but is short enough to avoid relaxation to thermal equilibrium. Remarkably, for many systems in nature this intermediate time scale is

very broad. During the fast dynamics of the system energy must be dissipated into the hidden degrees of freedom for the system to stabilize. Such energy dissipation is called hysteresis loss. In applications outside physics, hysteresis loss may acquire other meaning. In economic applications, for example, it will be the loss of wealth associated with decreasing the risk or payment of commissions.

2.2 Cyclic hysteretic trajectories

The general shape of hysteresis loops depends on system constraints and symmetry properties. Throughout most of this thesis we will consider systems with inversion symmetries. Systems with inversion symmetry are typical in magnetism, where the free energy is invariant with respect to changes in the sign of both the external variable (magnetic field) and the state (individual spin degrees of freedom). The results obtained for such systems can be easily extended to systems without inversion symmetry through the introduction of a constant bias in the external variable. However, it is not clear to what extent are the results applicable to systems where the state and the external variables are vector quantities.

A typical hysteresis loop for systems with inversion symmetry (magnetic systems), is illustrated by $M(H)$ relationship in Figure 2.3(a). H represents the external parameter (e.g. magnetic field), while M represents a response variable usually describing the average state of the system (e.g. magnetization). The $M(H)$ dependence is a multi-valued relationship for intermediate values of the control parameter, becoming single valued at saturation points obtained for sufficiently large magnitudes of H. The H/M variables are often referred to also as the input/output or the field/state variables. The loop obtained by increasing and decreasing the field H between the saturation points is called a major hysteresis loop. The points where the field direction is reversed are called reversal points (fields). If at least one of the reversal points

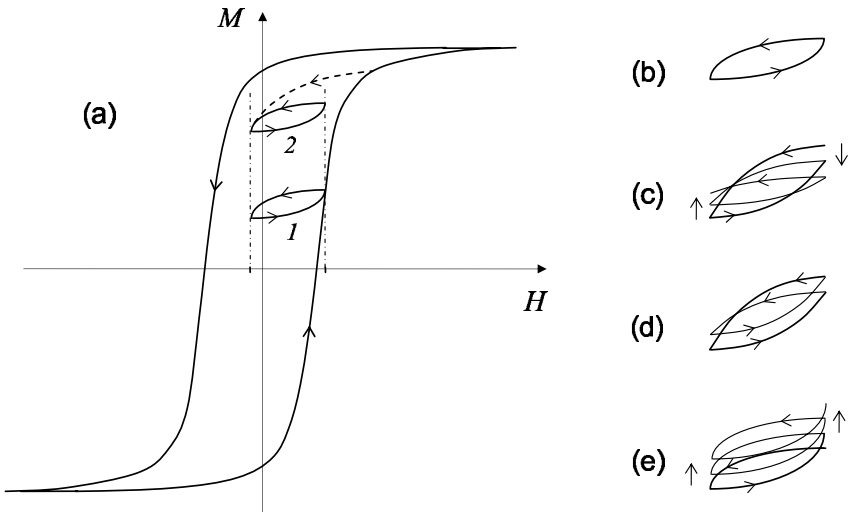

Figure 2.3: Minor cycle types. (a) Major hysteresis loop with two minor loops inside. Minor loops 1 and 2 correspond to the same reversal fields. (b) Closed loops: C-type cycles, (c) Tilting cycles: T-type cycles, (d) Cycles with subharmonic period: S-type cycles, (e) Drifting cycles; Reptation: R-type cycles.

is smaller then the saturation, then the field cycles produce minor cycles (loops) inside the major hysteresis loop. Examples of minor loops obtained for different field histories are illustrated in Figure 2.3(a). Minor loops 1 and 2 correspond to the same reversal fields but different previous history of the field variation. Closed loops shown in Figures 2.3(a-b) will be sometimes referred to as C-type cycles. Minor cycles, however, do not always form loops immediately after the first external field period and a number of periods might be necessary. Typical examples are illustrated in Figures 2.3(c-e). The trajectory shown in Figure 2.3(c), where the reversal points appear to move in the opposite directions will be sometimes referred to as T-cycles. Trajectories with both reversal points moving in the same direction, illustrated in Figure 2.3(e), will be called R-type cycles. Minor cycles with a multiple of the external field period are called subharmonic cycles, and will be referred to as S-type cycles (Figure 2.3(d)). In the following section we briefly review different classes of systems with hysteresis and classify their minor cycle behaviors whenever possible.

2.3 Examples of systems with hysteresis

1. Ferromagnetic materials. Ferromagnetic hysteresis has been well studied during the past century partly due to its technological importance for the magnetic information storage industry [1]. In most ferromagnets it is possible to freeze out thermal fluctuations at sufficiently low temperatures, and within a large range of measurement time scales the magnetization reversal processes can be viewed as independent of the measurement time. Thus, ferromagnets are very convenient for studying hysteresis. Various types of hysteretic behaviors have been observed depending on the interactions between the magnetic domains and the structural disorder present. Strict minor loop closure (i.e. C-type behavior in Figure 2.3) has been investigated by studying the repeatability of Barkhausen noise patterns [2,3] and using x-ray speckle metrology [4–6]. Gradually stabilizing minor cycles have also been observed [7–11]. Clean ferromagnets often exhibit T-type cyclic behavior called 'tilting' or 'bascule', which has been attributed to dipolar coupling between a few neighboring domains [12, 13]. Sufficiently disordered materials exhibit R-type cycles, the effect called 'reptation', which has been attributed to the interaction between a great number of domains [13–17].

2. Ordered magnetic nanostructures. In this case, the exchange interactions typical in ferromagnetic materials exist only within the nano-magnetic elements themselves. They are absent in the interactions between the elements of arrays, as the only interactions existing between individual magnetic elements composing the structure are the dipolar interactions. The strength and the sign of these interactions depends on the spacing and mutual orientations of individual elements. A review of the main properties of magnetic nanostructures as well as various processes used for their fabrication, such as lithography, self assembly, or growth methods, can be found in [18]. Hysteresis studies focused mostly on relating the effects of interactions to some features on the major loops. Relatively scarce minor loop measurements

revealed closed minor loops [19,20] in some cases. It has also been demonstrated that arrays of suitably arranged elements exhibit frustration effects (inability to satisfy all competing interactions which can be characterized using energy functional with many energy minima of about the same level) [21]. Frustration can be responsible for peculiar macroscopic effects, such as presence of hysteretic cycles with multiple periods (e.g. S-type cycles in Figure 2.3(d)) [22].

3. Exchange bias systems. Exchange bias effect results from quantum mechanical coupling between ferromagnetic and antiferromagnetic materials and is manifested as a shift (bias) of the hysteresis loop of the ferromagnetic material along the magnetic field axis. Despite the extensive research performed since the discovery of the exchange bias effect in 1956 [23], many of its aspects are still not fully understood [24, 25]. Observed hysteresis loops are often asymmetric [26, 27], even around the bias field value. In many systems, exchange bias reduces upon subsequent external field cycling and this behavior has been referred to as a training effect [28]. The training effect is similar to the R-type cyclic behavior illustrated in Figure 2.3(e), and has been attributed to partial reorientation of domains in the antiferromagnet with each reversal of the ferromagnetic layer. Training effects are absent for low symmetry antiferromagnets, such as antiferromagnets with uniaxial magnetic anisotropy [29]. Recently, exchange bias effect has been observed also in purely ferromagnetic bilayers [30, 31]. These structures may also exhibit training effects [32]. In addition, hysteretic behavior of the exchange bias itself has been discovered [33], and closed exchange-bias-hysteretic cycles have been predicted to exist for systems with negligible training effects [34].

4. Spin Glasses. Spin glasses are 'exotic' magnetic materials with ferromagnetic and antiferromagnetic interactions randomly distributed among magnetic moments [35]. Due to the mixed and highly disordered interaction structure, these materials exhibit strong frustration effects. Minor cycles typically display R-type behavior,

which however cannot always be completely attributed to the interplay between the interactions and disorder, and thermal effects must be included [7]. Modeling efforts demonstrated possibility of closed minor cycles in spin-glasses with long range interactions at low temperatures [36], and subharmonic S-cycles in spin glasses with short range interactions when strong frustration effects take place [37].

5. Type-II superconductors. In type-II superconductors, hysteresis results from the fact that as the external magnetic field changes, the flux filaments (vortices) move and their motion is pinned by defects such as voids, normal inclusions, dislocations, grain boundaries, compositional variations, etc. Interactions between the flux filaments are of electromagnetic nature [38, 39]. The resulting hysteresis behavior shows always closed minor loops as demonstrated experimentally [40, 41].

6. Rocks. Rocks like sandstone, igneous rocks or metamorfic rocks are examples of consolidated materials (a result of an assembly process) [42]. In these materials, individual grains act as rigid units and the contacts between them constitute a set of effective elastic elements (mesoscopic size cracks) that control the elastic behavior. When external stress is applied to such a composite system, elastic elements respond by opening or closing, depending on the magnitude of local pressure inside the rock, and produce hysteresis effects [43]. The hysteretic length vs. pressure relationship often displays closed minor loops [44, 45].

7. Capillary condensation. Capillary condensation of gasses adsorbed in disordered mesoporous materials refers to rapid change of a fluid inside the porous solid from a gas-like phase to a liquid phase [46]. Hysteresis is observed in sorption isotherms that measure the amount of fluid present in the solid as the pressure of the ambient vapor (or the chemical potential) is gradually increased and then decreased. Capillary condensation in various porous materials reveals asymmetric hysteretic loop shapes, where desorption (draining) occurs over a narrower range of pressures than adsorption (filling). While smooth hysteresis loops have been observed

in the low-porosity solids, in light aerogels the shape changed from smooth to rectangular as the porosity increased. Observed minor loops, however, remained closed in all cases [46–48]. It is interesting to point out that intersecting pores can be viewed as interacting via 'ferromagnetic-like' interactions, since an empty pore increases the probability of the intersecting pore being emptied as well. Different radii and cross-sections of the pores introduce disorder into the system. These observations have been used to develop unifying theoretical explanation of the capillary condensation phenomena in porous media [49–51].

8. Other systems. There certainly exist many other physical systems displaying hysteresis, such as irreversible processes in ferroelectrics, shape memory behavior in alloys, work hardening process in mechanical materials, contact angle hysteresis and so on. Over the past two decades, however, importance of hysteresis has been also recognized in complex systems of different nature. This includes economic systems, where a market share and the persistent states of unemployment, investment, and trade deficit strongly depend on history [52–55]. This also includes biological systems where the fate of a cell, tissue and, possibly, entire organism is determined not only by the current state of its environment, but depends critically on history of its development. The importance of such environmental effects and persistent memory of the past has long been debated in biology and medicine. Ability to pass the biological state of an organism to future generations through normal inheritance pathways makes the understanding of these developmental effects critical and is the subject of the growing field of epigenetics. Hysteresis has also been exploited in queuing systems such as modern information serving networks where significant switching costs are present. It would be difficult task to review all research in these fields and we refer the reader to excellent monographs dealing with this subject [56, 57].

Chapter 3. Hysteresis and network models

Various models have been developed to describe magnetic hysteresis, such as the Jiles-Atherton model, Stoner-Wolfharth model, and Globus model [1, 58, 59]. Models widely used also outside the area of magnetism are the Preisach models [60] and the Random Field Ising type models [57,61]. Since these two models are directly relevant for the purposes of this thesis, we will review their main properties in some detail below.

3.1 Preisach model and its properties

In the Preisach modeling, any hysteresis process is viewed as a superposition of switching events resulting from the flipping of independent bistable elements. Example of such element, typically called as 'relay', 'switch', or 'hysteron', is shown in Figure 3.1(a). Possible states are ± 1. While switching from the state -1 to state $+1$ takes place at the field $H = \alpha$, switching from the state $+1$ to -1 takes place at the field $H = \beta < \alpha$. If $H > \alpha$ then the relay is certainly in the $+1$ state, if $H < \beta$ then the relay is certainly in the -1 state. If $\beta < H < \alpha$, the state of the relay is determined by the previous external field history.

From the mathematical point of view, switches can be viewed as hysteretic operators acting on the input H and producing the output $+1$ or -1 depending on their inherent thresholds α and β, using the rules described above. Denoting such operators by $\hat{\gamma}_{\alpha\beta}$, the state of the system can be written as a superposition:

$$M = \int\int_{\alpha \geq \beta} \phi(\alpha, \beta) \hat{\gamma}_{\alpha\beta}[H(t)] \, d\alpha d\beta = \hat{P}[H], \tag{3.1}$$

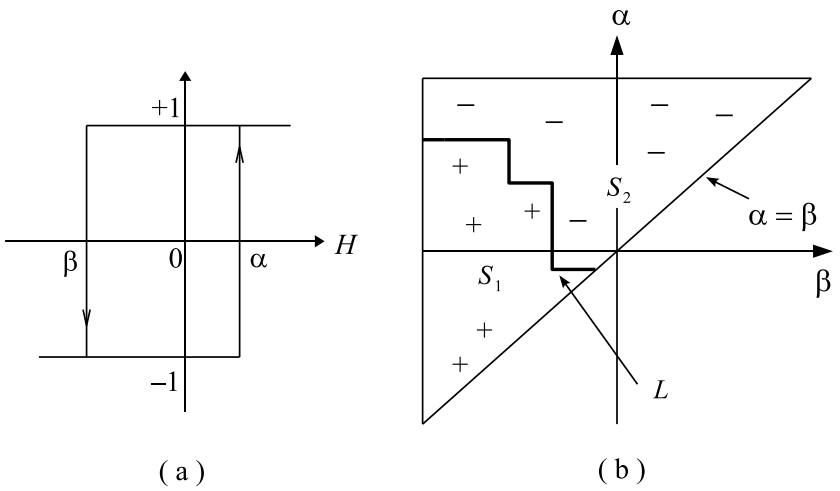

Figure 3.1: Preisach model. (a) Rectangular hysteresis loop of a relay - the basic building block of the Preisach model. Each relay with thresholds α and β corresponds to a point in the Preisach plane (b). The staircase interface line L separates regions with positively and negatively flipped relays, and its shape depends on the history of the applied field.

where $\phi(\alpha, \beta)$ is a weight function, called the Preisach distribution function, and defines a contribution of each relay to the overall magnetization. The integral in the Equation 3.1 is calculated over the half-plane $\alpha \geq \beta$. The functional relationship between M and H given by Equation 3.1 will be referred to as a Preisach operator $\hat{P}$.

To calculate hysteretic trajectories it is convenient to introduce a geometrical representation of Equation 3.1. There exists a one to one correspondence between the relays $\hat{\gamma}_{\alpha\beta}$ and the points (α, β) in the coordinate system defined by axes α and β. An illustration of such a (Preisach) plane is shown in Figure 3.1(b). We will assume that the support of the distribution $\phi(\alpha, \beta)$ is finite and bounded within a triangle defined by the line $\alpha = \beta$ and horizontal and vertical lines. The line L (discussed in more details below) defines interface between two regions S_1 and S_2 with respectively positively and negatively switched relays, for a given history of the external field H (see below). It is easily seen that Equation 3.1 can be written as a difference between

the integrals over the S_1 and S_2 regions:

$$M = \int\int_{S_1} \phi(\alpha, \beta)\, d\alpha d\beta - \int\int_{S_2} \phi(\alpha, \beta)\, d\alpha d\beta. \tag{3.2}$$

Wiping out and congruency properties. It will be discussed below that the classical Preisach model produces always closed minor loops. Consider a Preisach system evolving under the field monotonically increasing from the negative saturation where all relays are in the -1 state, to the point 1 on the major hysteresis loop as shown in Figure 3.2(a). As the field H increases, relays with thresholds $\alpha < H$ switch to the positive state. In the Preisach plane, the increasing field corresponds to the interface L being a horizontal line crossing the α-axis at the value H (Figure 3.2(b)). The areas below and above this line contain switches in the positive and negative states, respectively. Let us suppose that at the point 1 the field is reversed and starts to decrease. Positive switches with thresholds $\beta < H$ flip to negative states. In the Preisach plane, the decreasing field results in the addition to the interface L of the vertical line crossing the β-axis at the value H (Figure 3.2(c)). The region to the right contains switches which flipped back to the negative state, while the region to the left contains switches still in the positive state. When the field is reversed again at the point 2 and increases towards the point 1, the second horizontal part of the interface L moves up and the relays which flipped down during the decrease from 1 to 2 are being flipped back to positive state, until the original switch-state is completely recovered again at the point 1. This means that the minor loop generated between the points 1 and 2 must be closed. Further field cycles between the points 1 and 2 result in flipping of the same relays (those inside the triangle in Figure 3.2(d)) back and forth, and repeating the same loop. Similar behavior is shown in Figures 3.2(e-f) for a minor loop obtained by different field history, after first reversing the field at the point 3, decreasing it to the point 2, then increasing to 1 and decreasing back to

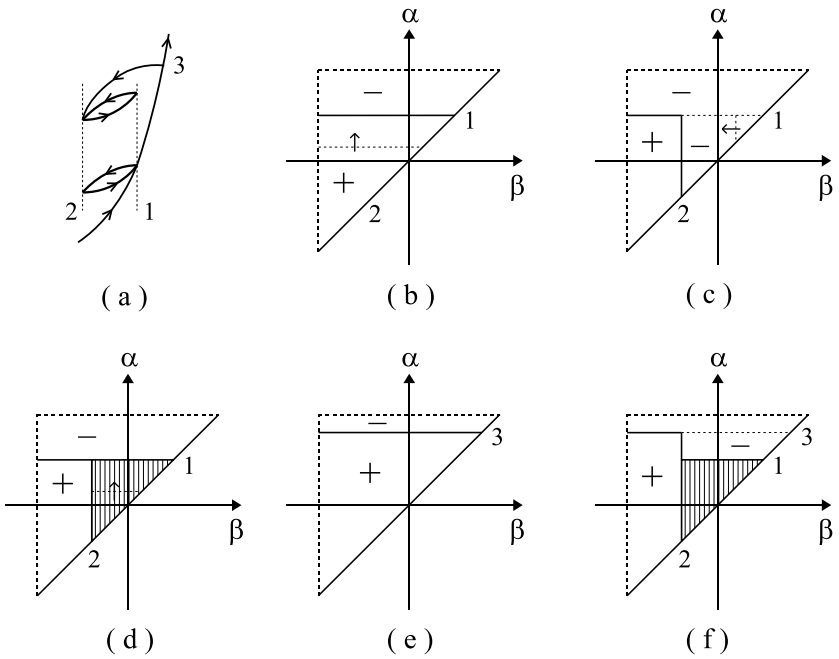

Figure 3.2: Wiping out and congruency properties of the Preisach model. (a) Two minor loops with the same reversal points 1 and 2 corresponding to different field histories. (b-d) Evolution of state on the Preisach plane during generation of a minor loop attached to the major hysteresis. (e-f) Generation of a minor loop with the same reversal fields obtained after first reversing the field at the point 3 on the major loop.

2. The resulting Preisach diagram producing the loop closure is illustrated in Figure 3.2(f). Note, that increasing the field back to the point 3 will also generate closed minor loop with reversal points 2 and 3. The loop closure is a general property of a Preisach model, which has been called 'wiping-out' or the 'return point memory'.

Another property of the Preisach model is the congruency property. Congruent loops are minor loops having the same reversal fields but corresponding to different field history, such that their geometrical shape is the same. The congruency property is the result of the fact that the triangular areas in Figures 3.2(c) and 3.2(f) corresponding to the same field extrema are identical. It is easily seen, by tracking the evolution of state on the Preisach plane, that switching regions obtained for the same reversal points will always be the same, independently of the number of pre-

vious reversal points. Thus, any pair of minor loops with the same reversal points will have the same shape and therefore be congruent. Congruency property is less fundamental than the wiping-out property. The wiping-out property is a consequence of the fact that the state of the model is the collective state of elementary operators each represented by a closed elementary hysteresis loop. Congruency property, on the other hand, is the result of expressing the output as a particular function of the state as specified by Equation 3.1. For other ways of expressing the output as a function of the state, no congruency will be observed. For example, Preisach model with a magnetization dependent input accounts for the non-congruency of minor loops [1,62] at least to some extend.

Preisach model is an example of a hysteretic system with interesting memory effects which result simply from the superposition of elementary bistable hysteresis loops. According to discussion in the previous paragraph it is clear that the coordinates of corners of the interface line L (e.g. Figure 3.1(b)) correspond to the upper and lower reversal points attained by varying external field. The staircase line L, therefore, stores information about the history of evolution of state of the system. Note, that due to the wiping out property, the entire information about the history of evolution is erased as soon as the external field increases above the largest extremum reached at a previous time.

It has been shown previously, that wiping out and congruency properties constitute the necessary and sufficient conditions which the system under study must satisfy if it is to be accurately represented by the Preisach model [63]. The Preisach distribution $\phi(\alpha, \beta)$ can then be uniquely identified from a set of straightforward macroscopic measurements [63], and Equation 3.2 can be used to predict magnetization curves for any sequence of external field extrema. Finally we note that the classical Preisach model does not reproduce many hysteretic behaviors observed in real systems, such as gradually stabilizing minor loops. Many modifications have been introduced to

account for such effects. Preisach models with gradually stabilizing cycles have been developed and discussed in detail in [10]. Rate dependent hysteresis effects have also been modeled using modified classical Preisach models [64]. Another class of hysteresis models are the vector Preisach models where both the input and the output variables are of a vector nature [65–68].

3.2 Random Field Ising model (RFIM)

The discussion in the previous section reveals phenomenological nature of the Preisach model. Indeed, hysteretic relays - the basic building blocks of the Preisach model need not to be associated with physical parts of the system and still reproduce macroscopic hysteresis measurements. In fact, they often have to be viewed as abstract mathematical objects. Different approach to hysteresis modeling is to divide the system into basic components, such as magnetic domains or capillary pores, for example, and explicitly specify interactions between them. Then, after defining the Landau free energy for the system and the rules governing the evolution of state, dynamical behavior under varying external conditions can be studied. A prototypical model for studying hysteresis using this framework is the Random Field Ising model [57, 61].

In its original definition, Random Field Ising model (RFIM) has been viewed as a collection of ± 1 non-hysteretic elements, called spins, distributed on the D-dimensional lattice. Spins interact with their neighbors on the lattice and with the external field H. In addition, every spin is exposed to some quenched (fixed) field which can be viewed as a source of disorder in the system. In the RFIM, these quenched fields are assumed to vary from site to site on the lattice. The total energy determining the switching of each spin is given by the sum of spin-spin, spin-external-field, and spin-quenched-field interaction energies. During the external field H variation, spin states are updated at each time step to minimize the total energy.

If the interactions are such that parallel alignment of spins is favored (e.g. positive exchange interactions in ferromagnetism), then the spins flipping at a given instant of time can trigger also neighboring spins to flip. Such events can propagate throughout the system and result in avalanches. Due to such behavior, which is not explicitely present[1] in the Preisach model described in previous section, the RFIM has been used as a paradigm for studying noise statistics in various out of equilibrium systems, such as Barkhausen noise in magnets, frequency of occurrence of earthquakes, or acoustic emission bursts generated during martensitic transformations [69]. It has been shown that reducing the disorder relative to the spin-spin interaction strength results in the increase of the average avalanche size. At a certain critical disorder level, infinite avalanches spanning entire system emerge, and a steep jump appears in the originally smooth hysteresis loop [70]. This disorder induced phase transition has been studied in detail using the renormalization group techniques [69, 71], with the main emphasis on identifying various scaling relations, critical exponents, and determining the universality class of the RFIM. In addition, the ferromagnetic RFIM has been shown to have a return point memory (wiping out property) and consequently produces always closed minor cycles [70]. Unlike in the case of Preisach model, however, the congruency property does not hold in general.

The RFIM model has been investigated in the contexts of many systems of differing natures, with either uniform or random interaction magnitudes between the spins, interactions of different signs, different topological arrangements of spins, various types of disorder, etc. This work is briefly reviewed in the following section where we refer to this type of models jointly as 'binary spin networks'.

---

[1] It is present implicitly through the Preisach distribution function.

3.2.1 RFIM-type modeling of hysteresis: A brief review

Binary spin networks have been used as paradigms for studying hysteresis processes in magnetic, ferroelectric and non-elastic materials, living organisms, social and economic structures and many others. An example is the RFIM model with spins distributed on a regular lattice discussed in the previous section, which has been used to model the noise statistics produced during the field-driven hysteresis processes and revealed an existence of disorder induced non-equilibrium phase transitions [57, 61]. Employing the RFIM with spins on a Bethe lattice, and on a random network, such phase transitions have subsequently been shown to depend on the spin coordination number, i.e. on the connectivity of the spin network [72–74]. In addition, it was demonstrated that variations in the connectivity and the structural inhomogeneity of the network are responsible for avalanches and hysteresis loop criticality also in random networks with negative (antiferromagnetic-like) interactions between the spins [75]. Such behavior is absent for regular lattice antiferromagnetic networks [76, 77]. Spin glass networks, where the interactions between neighboring spins have a random sign and magnitude [35], have been shown to exhibit signatures of frustration and of self-organized criticality (self-organized criticality refers to behavior where the system rests at a critical point naturally, without the need to tune external conditions) [36]. Among other examples of spin networks are Random Bond Ising model, Site Diluted Ising model, Random anisotropy Ising model and others [78].

Evolution of state of the network subject to adiabatic cycles of the external input has also been considered and led to discoveries of interesting memory effects. The return point memory yielding always closed minor loops, frequently observed in ferromagnetic spin networks, has also been observed in some antiferromagnetic networks [79, 80]. A 'complementary point memory', where two complementary points on the major hysteresis (i.e. points related by inversion symmetry around the coordi-

nate origin) have identical microstates, has been observed in spin glass networks with short range interactions at non-zero temperature [81]. Studies of spin-glass networks also led to discovery of the 'reversal field memory' where a certain reversal curve inside the major hysteresis loop appears to remember the negative of its reversal field. This memory effect has been shown to be due to the local spin-reversal symmetry of the associated Hamiltonian [82]. Only a few works dealing with analysis of systems displaying a gradual convergence to minor loops and multi-cycling behavior seem to be available [22,37,80,83,84]. Such studies typically employed regular-lattice spin networks with antiferromagnetic and magneto-static interactions. Among many questions remaining to be answered are: What is the effect of interactions versus the disorder on the hysteresis cycles? How does the connectivity of the network influence the rate of a minor loop formation? Are topological features of the network important? It is the task of this thesis to seek answers to these questions.

3.3 Random networks: Elements of the graph theory

In this section we describe some main properties of networks, which will be used throughout this thesis. Mathematical objects convenient for describing the structure of the interaction network, i.e. the distribution of interaction links among the spins, are called *graphs*. A graph is defined as a set of N points (nodes, vertices) and n links (lines, edges) interconnecting pairs of points. It is fully characterized by the associated $N \times N$ adjacency matrix A, with elements $A_{ij} = 1$ if two vertices i and j are connected or $A_{ij} = 0$ if not. Excluding the parallel edges (melons) and edges from node to itself (talons), there are total $N(N-1)/2$ possible edges in the graph on N points and, therefore, there exist $C^n_{N(N-1)}$ different graphs having a total of n edges distributed among the points. The number of edges emanating from the node i defines a degree of that node, d_i, and it holds that $d_i = \sum_j A_{ij}$. The average degree of the

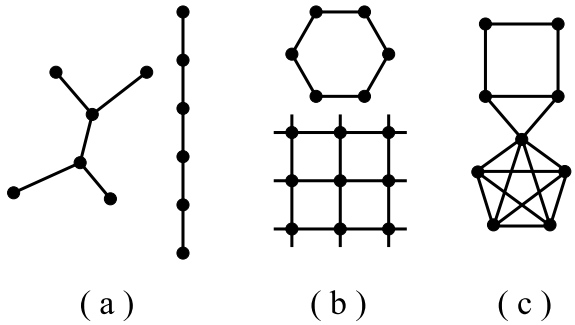

Figure 3.3: Examples of various graph structures: (a) Trees of the order $k = 6$. A linear chain of spins can be represented by a tree like graphs. (b) Cycle of order $k = 6$. The square lattice contains cycles of different orders starting from $k = 4$. (c) Complete subgraphs of order $k = 3, 4, 5$.

network is $d = \langle d_i \rangle = N^{-1} \sum_{ij} A_{ij}$. Any set of nodes and edges chosen from the graph defines its subgraph. Graphs (subgraphs) can assume various topological structures. Examples are cycles, trees or complete subgraphs. A cycle of order k is defined as a closed loop of k edges such that every two consecutive edges, and only those two, have a common node (Figure 3.3(b)). A tree of order k is a connected graph with k points and $k - 1$ edges such that none of its subgraphs is a cycle. Examples are shown in Figure 3.3(a). Note that a linear chain of spins can be viewed as network with a tree like structure having $d = 2$, and that a two-dimensional lattice of spins with $d = 4$ contains also cycles (Figure 3.3(b)). A complete subgraph of order k (often referred to as clique of size k) is a set of k points where each point is interconnected with every other point. Example in Figure 3.3(c) contains total 15 complete subgraphs of order three, 5 subgraphs of order four and 1 subgraph of order five.

3.3.1 Classical random graphs (Erdös-Rényi)

Complex networks with often unknown organizing principles and complex topology frequently appear random [85]. A convenient mathematical framework for studying such objects is the random graph theory, which deals with graphs with a randomly

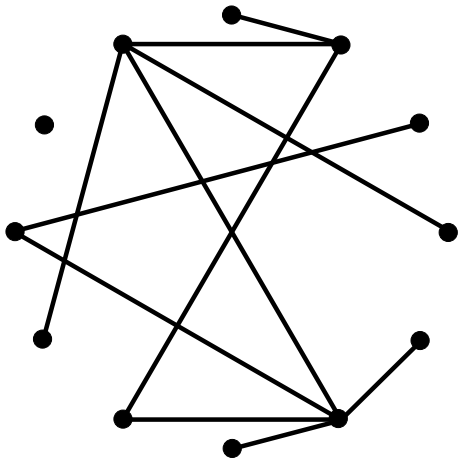

Figure 3.4: Erdös-Rényi random network having 12 nodes and 11 edges.

varying degree d_i (Figure 3.4). Among well understood are the classical random graphs, also called Erdös-Rényi graphs [86], which are constructed by adding n edges, one by one in n steps, to the randomly chosen pairs from N spins. An equivalent process is to assign a link between every spin couple independently with probability p. The main properties of Erdös-Rényi (ER) graphs are summarized below. Our discussion follows [87].

In an Erdös-Rényi random graph with connection probability p, the degree d_i is a random variable following binomial distribution with parameters $N-1$ and p:

$$P(d_i = q) = C^q_{N-1} p^q (1-p)^{N-1-q}. \tag{3.3}$$

The probability P describes a number of ways in which q edges can be drawn from a node i. If i and j are two different nodes, then $P(d_i = q)$ and $P(d_j = q)$ are close to being independent random variables (not entirely independent because removing the node i can affect degree of the node j if they are connected, especially when the system size is small).

It can also be shown that the probability distribution to find X_q nodes having the

degree q follows a Poisson distribution [87]:

$$P(X_q = r) = e^{-\lambda_d} \frac{\lambda_d^r}{r!}, \tag{3.4}$$

where λ_d denotes the expectation value of the number of nodes with degree q. Using Equation 3.3 it follows that $\lambda_q = \langle X_q \rangle = NP(d_i = q)$ and λ_q thus depends on q, p, and N. Since the standard deviation equals $\sigma_q = \lambda_q^{1/2}$, the Poisson distribution decays rapidly for large values of r, and it is reasonable to approximate $X_q \approx \langle X_q \rangle = \lambda_q$ (valid if the nodes can be viewed as independent). The degree of each node is, therefore, approximately the same and Equation 3.3 can then be rewritten as:

$$P(q) = C_{N-1}^q p^q (1-p)^{N-1-q}, \tag{3.5}$$

which for $N \to \infty$ reduces to a Poisson distribution:

$$P(q) = e^{-pN} \frac{(pN)^q}{q!} = e^{-\langle d \rangle} \frac{\langle d \rangle^q}{q!}. \tag{3.6}$$

The last equality has been obtained by using Equation 3.4 and the fact that for large N the $\lambda_d \approx d$. The considerations above suggest that a typical random graph is rather homogeneous, with the majority of the nodes having the same number of edges. Equation 3.6 shows that for a large number N of vertices in the graph, the connection probability and the average degree are related as $d \approx pN$. Since $d = 2n/N$, the probability p can be related to the number of edges n as $p \approx 2nN^{-2}$. Note that if the system size N increases while d is held fixed, p has to necessarily decrease.

3.3.2 Emergence of subgraphs in the Erdös-Rényi network

The connectivity and the topological structure of the random network depend on the link-probability p. As p increases, many properties of the graphs such as appearance

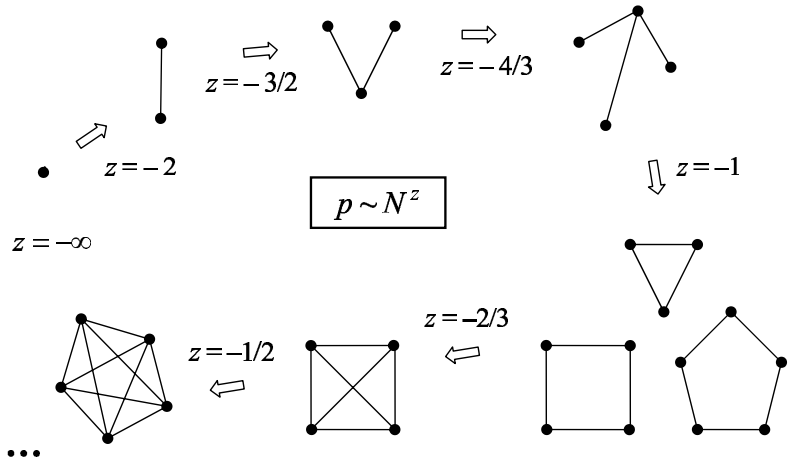

Figure 3.5: Evolution of a graph structure. Different topological elements appear suddenly at specific probabilities p.

of trees, cycles, or cliques emerge suddenly at some critical probability P_c, similarly to phase transition behavior occurring in physical systems [88]. The values of P_c depend on the network size N. It is convenient to express the dependence of probabilities on the network size as a power law $p \approx N^z$, where z is a tunable parameter varying between $-\infty$ and 0, and then follow the evolution of a graph structure as z increases (Figure 3.5). For $z < -3/2$ almost all graphs contain only isolated nodes and edges. When z passes through $-3/2$, trees of order 3 suddenly appear. Trees of order 4 appear as soon as z exceeds $-4/3$. As z approaches -1, graph contains trees of larger and larger order. However, as long as $z < -1$ which means that average degree of the graph $d = pN \to 0$ as $N \to \infty$, the graph is composed only of disconnected trees. When z passes through -1, the asymptotic probability of cycles of all orders jumps from 0 to 1, even though z is changing smoothly. Note that cycles of order 3 can also be viewed as complete subgraphs of order 3. Complete subgraphs of order 4 appear at $z = -2/3$, and as z continues to increase, complete subgraphs of larger and larger order emerge. As $z \to 0$ almost every random graph approaches a complete graph of size N.

It has also been shown that there exists an abrupt change in the cluster structure of a random graph as $d \to 1$. For $d < 1$ there are relatively few edges and all components (subgraphs) are small, having an exponential size distribution and a finite mean size. However, when $d \geq 1$, an extensive fraction of all vertices are joined together in a single giant component and graph becomes well connected.

Chapter 4. Random Coercivity Interacting Switch model (RCIS)

The Preisach and the RFIM models do not reproduce certain experimental observations, such as the T and R cycles illustrated in Figure 2.3. Although there exist modifications of the Preisach model which account for the R-type cycles [10], they are purely phenomenological and do not yield information about the nature of the cycle opening and its relation to the structure and the disorder in the system. On the other hand, while the RFIM with positive interactions (ferromagnetic) has strict return point memory property [70], and thus always closed minor loops, the RFIM model with negative interactions displays only almost negligible hysteretic effects [76].

For these reasons we developed different physically motivated model, called Random Interacting Switch model (RCIS), which reproduces these aspects of hysteresis not seen in the Preisach or RFIM models, and allows studying the relationship between the types of minor cycles and the structure of interactions and disorder.

4.1 Definition

The Random Coercivity Interacting Switch model (RCIS) combines the Preisach model and RFIM discussed in Sections 3.1 and 3.2. It is a collection of N interacting spins s_i, with $+1$ or -1 being the only allowed states. Switching of each spin is described by a rectangular hysteresis loop with symmetric thresholds $\pm\alpha_i$, $\alpha_i > 0$. The thresholds α_i are viewed as random variables with probability distribution $\rho(\alpha)$, and mimic structural disorder in the system. Such classical hysteretic spins are frequently used as representations of single domain magnetic grains, tiny capillary pores in absorbing materials, vortex pinning imperfections in superconductors, individual decision making agents in socio-economic systems, etc. [57].

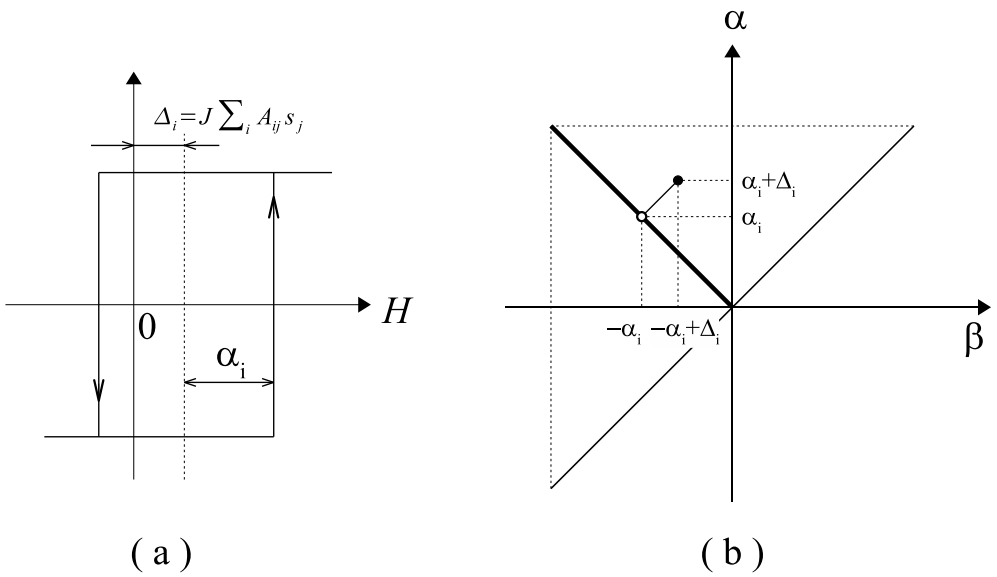

Figure 4.1: (a) Rectangular hysteresis loop corresponding to the switch s_i with symmetric thresholds α_i and $\beta_i = -\alpha_i$, shifted from the coordinate origin due to the interaction with the neighboring spins. (b) When the interaction is equal to zero, all spins with symmetric thresholds lie in the Preisach plane on the line perpendicular to $\beta = \alpha$ line. For nonzero interactions, both thresholds are shifted by an amount Δ_i, which depends on the interaction strength and on the state of the neighbors of the spin s_i.

The spins s_i and s_j will be assumed to interact via pair-wise interactions described by a matrix $J_{ij} = \delta J A_{ij}$, where J is a positive constant representing the interaction strength, δ equals either $+1$ or -1 depending on whether the system is of ferromagnetic or antiferromagnetic nature (i.e. if parallel or anti-parallel alignment of neighboring spins is preferred). The matrix A_{ij} is $N \times N$ adjacency matrix of the associated graph, with elements $A_{ij} = 1$ if the spins s_i and s_j interact and $A_{ij} = 0$ if they do not interact, and describes topological structure of interactions.

In the absence of interactions, spins flip whenever the external field H matches their switching thresholds. Generally, however, the flipping of any spin s_i will be determined by a local field h_i, dependent on the external field and also on the contribution from interactions of s_i with other spins. We assume that h_i can be written

as a sum:

$$h_i = H + \sum_{j=1}^{N} J_{ij} s_j = H + \Delta_i \tag{4.1}$$

where the symbol Δ_i denotes an interaction field due to the neighbors of s_i. Δ_i determines a shift of the originally symmetric rectangular loop with thresholds $\pm\alpha_i$ from the coordinate origin (Figure 4.1(a)). This shift can also be depicted in the Preisach α-β plane, as shown in Figure 4.1(b). To any spin s_i with symmetric thresholds, there corresponds a point $(-\alpha_i, \alpha_i)$ on the line $\alpha = -\beta$ in the α-β plane. When the interaction field Δ_i is nonzero, this point is shifted to $(-\alpha_i + \Delta_i, \alpha_i + \Delta_i)$. As the system evolves and neighboring spins flip back and forth, the Δ_i changes and the points in the plane change their position accordingly. It is easy to see, following the rules introduced in Section 3.1 and Equation 4.1, that the points in the Preisach plane move along with the external field H line if the interactions are negative (antiferromagnetic), and they move against the field if the interactions are positive (ferromagnetic). Due to the presence of disorder and nontrivial interaction topologies, details of this motion are complicated, often resulting in a breaking of the return point memory and the congruency properties. This demonstrates the difference between the RCIS and Preisach models.

4.2 Adiabatic dynamics

The spin state of the system remains stable as long as the local fields of all spins remain greater or smaller then their upper and lower thresholds, i.e. as long as $h_i s_i > -\alpha_i$ holds for any spin s_i. As the external field H evolves, h_i changes according to Equation 4.1. Flipping occurs as soon as $h_i s_i < -\alpha_i$, and the evolution of the system towards the next stable state proceeds according to the following rules:

R1. In a pre-defined order, update the state of every relay one at a time according

to:

$$s_k(n+1) = \begin{cases} +1 & \text{if } h_k(n) \geq +\alpha_k \\ -1 & \text{if } h_k(n) \leq -\alpha_k. \\ s_k(n) & \text{otherwise} \end{cases} \tag{4.2}$$

$\underline{R2}$. If all relays end up in the stable state go to $R3$, otherwise repeat $R1$.

$\underline{R3}$. Increment the input H by the smallest possible amount ΔH required to induce switching of at least one relay s_i in the RCIS network.

In general, the steps $R1$ and $R2$ need to be repeated a number of times until the stable state of the RCIS is reached. While the state of the RCIS varies during this stabilization, the external field H remains fixed. Such relaxation process mimics many behaviors known in the physical sciences, such as a Barkhausen jump (magnetism) or an avalanche (earthquake), for example. Moreover, the relationship between the input and the stable state of an RCIS network (or any function of it) is the same regardless of the rate of input variation and therefore the dynamics $R1-R3$ produces rate-independent hysteresis behavior. The dynamics $R1-R3$ is often used to model processes when thermal fluctuations are absent, and is often referred to as a field driven adiabatic (zero-temperature) dynamics [70].

4.3 Convergence to the stable state

To prove that repeated iterations of steps $R1-R2$ converge to a stable state, it is convenient to define the state function based on the analogy with the RFIM:

$$G = -\frac{1}{2}\sum_{ij} J_{ij}s_i s_j - H\sum_i s_i. \tag{4.3}$$

The first term in the Equation 4.3 is the spin-spin interaction energy, while the second term describes the interaction of individual spins with the external field. We

now observe that:

$$-\frac{\Delta G}{\Delta s_i} = H + \sum_{j=1}^{N} J_{ij} s_j = h_i, \tag{4.4}$$

where h_i is the local field defined by Equation 4.1. The switching rule $R1$ implies:

$$0 < h_i \Delta s_i = -\frac{\Delta G}{\Delta s_i} \Delta s_i = -\Delta G. \tag{4.5}$$

Since only one relay can be switched at a time n, the state function G necessarily decreases during any switching event. Moreover, G is always bounded from below, and thus the switching process $R1 - R2$ must terminate after reaching a local minimum of G.

The function G can be viewed as a free energy function of the RCIS network. It is important to note, that there is also a double well free energy associated with individual hysteretic spins. Due to the symmetry of thresholds of spins, however, this free energy is the same in their negative and positive states, and its addition in Equation 4.3 would only add a constant that would not affect any further results. This argument does not hold for non-symmetric relays, which will not be considered in this work.

4.4 Single spin flip dynamics limit

According to Section 4.2, avalanches are multiple switching events consisting of many spins flipping at a given field. If during the step $R1$ more then one spin becomes unstable, then we flip all unstable spins in a predefined sequence starting from the spin with the largest sum $h_i s_i + \alpha_i$ (force). However, are the resulting stables states independent of the actual order in which the unstable spins are updates? Or in other words: Do different updating sequences produce the same state of the system? As it turns out, the same final state is obtained independently of the order of updating only

if the interactions are positive $J_{ij} > 0$ [74]. If the interactions are negative $J_{ij} < 0$, different final states are obtained depending on the order of the flipping the spins [77]. The procedure for choosing the correct order of updating in this case remains unclear.

This issue can be partially resolved in the present RCIS model. In the low interaction limit, the dynamics $R1 - R3$ introduced in Section 4.2 reduces to a very simple regime with trivial avalanches consisting of single spin flips only. The argument is as follows. While avalanches in the ferromagnetic RCIS consist of spins always flipping along the external field direction (i.e. $\Delta H \Delta s_i > 0$), in the antiferromagnetic case avalanches are nontrivial and can contain spin flipping both ways, along and against the external field direction. Due to the antiferromagnetic interactions, the local fields on the neighbors of some spin s_i flipping along the field H become reduced. If the interaction magnitude J is sufficiently large, then such a decrease of local fields may trigger some of these neighbors to flip against the field H. As it turns out, however, there exists an interaction limit, J_t, such that back-flips must be absent as long as $J < J_t$. Denoting the minimum threshold magnitude from among all spins in the system by $\alpha_{\min} = \min(\alpha_i)$, the maximum degree (the degree of a node equals to the number of links emanating from it; Section 3.3) present in the network by $d_{\max} = \max(d_i)$, and given the Equation 4.1, the backward transitions will clearly be impossible in the RCIS if $\max(\Delta_i) = \max(d_i) J |s_i| < \alpha_{\min}$. This relation defines the limiting interaction magnitude:

$$J_t = \alpha_{\min} / d_{\max}. \tag{4.6}$$

For $J < J_t$ the back-flips will be absent, the avalanches trivial, consisting of single spin transitions when $\Delta H \Delta s_i > 0$, and the state dependence will be a monotonic function of external field H. In fact, this behavior is realistic for magnetic films with very strong perpendicular anisotropy for example [18, 89].

In this thesis we will often employ a Gaussian distribution of thresholds. The mean and the variance of the distribution will be denoted respectively by μ and σ, and we will always assume that $\mu >> \sigma$. Truncating the thresholds α_i below $\alpha_{\min} = \mu - 3\sigma$, when the probability for observing $\alpha_i < \alpha_{\min}$ becomes negligible, allows specifying the weak interaction limit using Equation 4.6 as:

$$J_t = (\mu - 3\sigma)/d_{\min}. \tag{4.7}$$

Note that due to the truncation of the random thresholds below $\alpha_{\min}$, the threshold distribution slightly differs from the Gaussian. We also considered other distributions, including log-normal and uniform, which all yielded results qualitatively similar to those presented in this thesis.

4.5 Summary

In this chapter we defined the RCIS model which will be used next to investigate behavior of cyclic trajectories and their relation to the structure of interactions and disorder. The RCIS model can be viewed as a combination of the Preisach and RFIM models. Its main new property, when compared to previous models, is the single spin flip dynamical limit which allows thermodynamically consistent analysis even in the case of negative interaction networks. As will be shown in this thesis, RCIS model reproduces many qualitative features of hysteresis observed in nature.

Chapter 5. Mean field models: From closed to open cycles

In this chapter we use the RCIS model to investigate origins of the cycle opening. We show that networks with positive (ferromagnetic) interactions produce always closed minor loops. This is due to the return point memory property (RPM), which will be shown to hold for ferromagnetic networks of an arbitrary adjacency matrix. No such general statements can be made about networks with negative interactions (antiferromagnetic), and in fact antiferromagnetic networks generally do not produce closed cycles. However, there are some cases where the RPM still holds. As an example we discuss mean field RCIS model with spins on a fully connected network. We then show that a modification of such system obtained by dividing the interaction network to form two interacting mean field RCIS models produces new behavior, where open cycles emerge suddenly at some critical interaction. This result suggests that both the RPM (Figure 5.1A(a-b)) and the cycle opening (Figure 5.1B(a-b)) could be observed in some antiferromagnetic networks, depending on their structural parameters.

5.1 Cycle closure in the positive interaction networks: Return Point Memory (RPM)

The fact that the RPM property holds for RCIS model with positive interactions can be shown similarly as demonstrated previously for the ferromagnetic RFIM model [70]. Only a few straightforward modifications need to be introduced, which account for the hysteretic nature of spins and the fact that we consider networks with an arbitrary adjacency matrix.

Assume a spin network with adjacency matrix A_{ij} and the spin-spin interaction strength $J > 0$. Let any two spin states of the system be denoted by the vectors

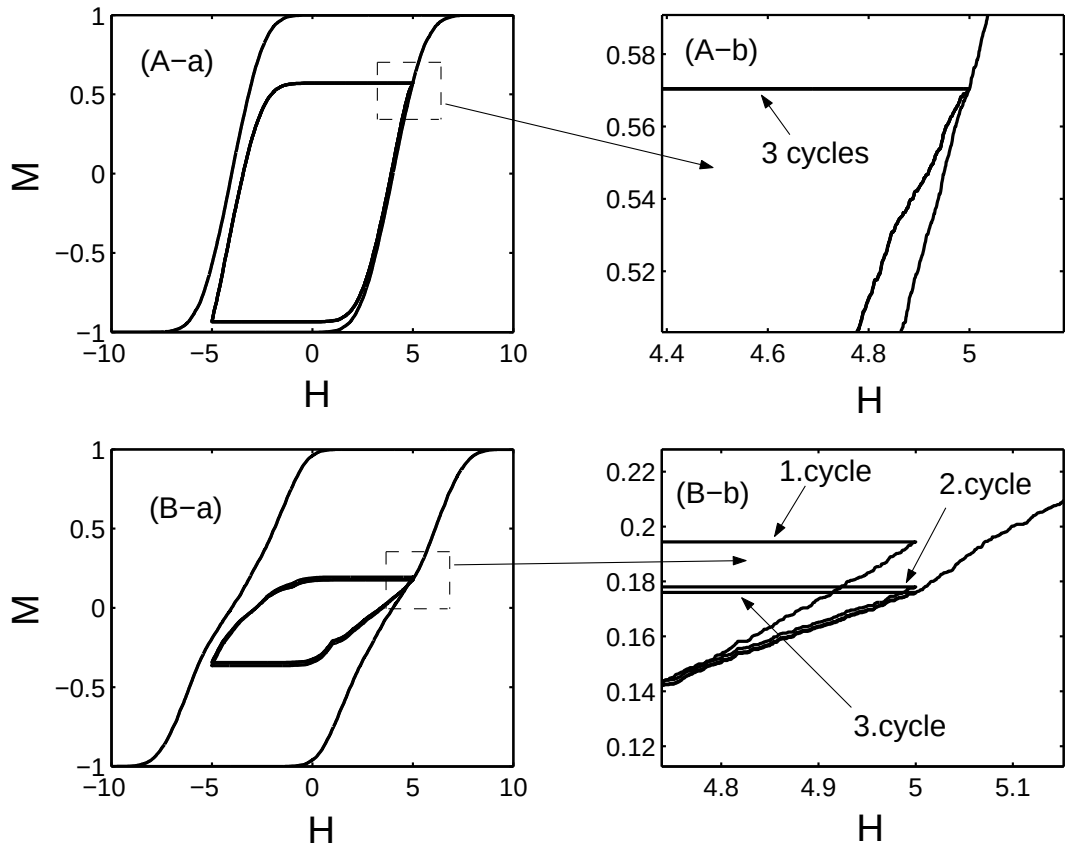

Figure 5.1: A(a-b) Minor loop cycled 3 times showing complete closure at the end of the first cycle for interaction weaker than the critical point. B(a-b) 3 minor cycles showing opening for interaction stronger than the critical point.

$s = \{s_1, s_2, \ldots, s_N\}$ and $z = \{z_1, z_2, \ldots, z_N\}$. The states s and z will be called *partially ordered* if $s_i \geq z_i$ for every i (or if $s_i \leq z_i$ for every i). One very important property of ferromagnetic networks is that the partial ordering of states remains preserved under the field driven adiabatic dynamics defined in Section 4.2. If the spin states s and z attained respectively at fields H_s and $H_z \leq H_s$ are ordered at some initial time, then their ordering will remain preserved under the field variation as long as the condition $H_z \leq H_s$ holds.

The proof of this property follows by reaching the contradiction. Assume the ordering $s \geq z$, which holds at some initial time for $H_s \geq H_z$. This partial order would

be violated as soon as some spin z_i flips before s_i anytime during the evolution under $H_s \geq H_z$. Observe, that if the spin z_i is to flip before s_i (i.e. if $s_i \leq z_i$ is to happen) at some instant of time, the corresponding local fields given by Equations 4.1-4.2 must at that time satisfy the inequality:

$$h_i^s = J \sum_j A_{ij} s_j + H_s \;\leq\; h_i^z = J \sum_j A_{ij} z_j + H_z. \tag{5.1}$$

However, since 1) $H_s \geq H_z$ holds by requirement, 2) $J \sum_j A_{ij} s_j \geq J \sum_j A_{ij} z_j$ because all neighbors around the node i still remain ordered at that time instant, and 3) noting that both z_i and s_i are at the node i and therefore have the same threshold α_i, then any event yielding $s_i \leq z_i$ is impossible. Thus the partial order remains preserved under the dynamics at all times. The above argument holds for any adjacency matrix A_{ij} of the network as long as J remains positive.

The preservation of partial ordering and the adiabatic dynamics condition (Section 4.2) guarantee that the final state of the system, which evolves under an external field arbitrarily changing between two limits (bounds), depends only on the final value of the external field. The final state does not dependent on the duration of the field variation or on the history, as long as the field remains within the bounds. As a consequence, minor cycles obtained by cycling the field between two reversal points must recover the same spin state after each cycle, demonstrating the RPM. The proof of this property is identical as for the RFIM and details can be found in [70]. The RPM is a remarkable property that seems to hold in many systems in nature. Several examples, such as e.g. ferromagnets, type-II superconductors, and capillary condensation in porous media can be found in Section 2.3.

5.2 Cycle closure in the negative interaction networks

The proof of the RPM for the RCIS given in the previous section applies only to the positive interaction case. However, RPM holds also for some specific networks with negative interactions. As an example of such an antiferromagnetic system, we consider an RCIS model with spins on a fully connected network. Since systems with fully connected interaction networks are typically called mean field models, we adopt the same terminology. Minor loop behavior in the mean field RCIS model has been studied previously in the context of the moving Preisach model [90], and the RPM property has been shown to hold for both positive and negative interactions [62]. Here we present alternative (informal) argument demonstrating the RPM property in the mean field RCIS model.

For a fully connected interaction network, all off-diagonal elements of the $N \times N$ adjacency matrix are equal to 1, and according to Equation 4.1, the local fields h_i can be expressed as

$$h_i = H - J'M, \tag{5.2}$$

where $J' = NJ$, $M = N^{-1}\sum_j s_j$ is the average state of the system (magnetization) and the '$-$' sign is due to the antiferromagnetic nature of interactions. Note that since h_i is the same for every spin, the state of spins depends only on the variables H and M, or more precisely, on the difference $H - J'M$. The functional dependence of the spin's state can be expressed as $s_i = s_i(H - J'M)$ and the magnetization as:

$$M = \frac{1}{N}\sum_i s_i(H - J'M) = \hat{P}[H - J'M], \tag{5.3}$$

where $\hat{P}$ is a Preisach operator introduced in Section 3.1. Note that the Preisach operator in Equation 5.3 depends also on the output variable M. For this reason the model defined by Equation 5.3 has been called moving Preisach model [90].

The RPM can be demonstrated as follows. Consider the single spin flip dynamics limit defined in Section 4.4. The back-flipping spins do not exist then, the difference $H - J'M$ increases (decreases) whenever the external field H increases (decreases), and the dependence of M on H given by Equation 5.3 must be monotonic (i.e. $\Delta M \Delta H \geq 0$). Consequently, the operator relationship:

$$H = \hat{P}^{-1}[M] + JM = \hat{\Gamma}[M] \tag{5.4}$$

obtained by inverting the Equation 5.3 must also be monotonic. Since the closed loops generated by a monotonic hysteresis relationship map into closed loops of its inverse, the Preisach model $\hat{P}^{-1}$ also exhibits the RPM. The addition of the linear term $J'M$ in Equation 5.4 does not change this fact since it only tilts the hysteresis loops. Thus, the operator $\hat{\Gamma}$ has the RPM and monotonicity properties, implying the same for its inverse $M = \hat{\Gamma}^{-1}(H)$.

Note, that if the above argument holds for any network size N, then also the ensembles of spins forming couples, cycles of size 3, and cliques of any size will have the RPM property, and therefore display closed cycles.

5.3 Néel's mean field model: Transition between RPM and open cycles

Consider two groups of spins, such that the spins within each group do not interact with each other. This situation is illustrated in Figure 5.2, where the spins on the lattice are divided into two interpenetrating sub-lattices A and B. Magnetizations (average states) of each sub-lattice are M_a and M_b and the total magnetization in the system is an average $M = (M_a + M_b)/2$. While the spins within the sub-lattice do not interact with each other, every spin s_i^A from sub-lattice A interacts with all spins s_i^B from the sub-lattice B via the same mean field $-J'M_b$, and every spin s_i^B from sub-lattice B interacts with all spins from sub-lattice A via the mean field

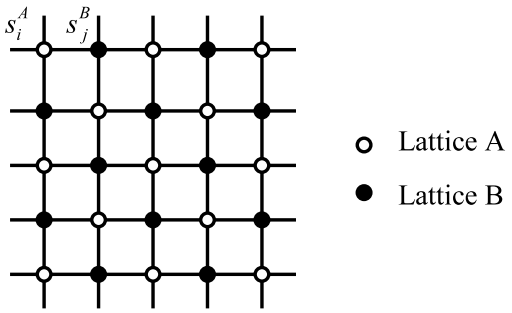

Figure 5.2: Néel's lattice. Shown are two interpenetrating lattices A and B (white and black dots) of spins. Magnetizations of each sub-lattice are M_a and M_b. Spins do not interact within the sub-lattice. Interaction is only between the spins from different lattices via the mean fields $-J'M_a$ and $-J'M_b$, where J' is the interaction magnitude. Magnetization of the entire system is an average $M = (M_a + M_b)/2$.

interaction $-J'M_a$ ($J' > 0$). This structure of interactions is analogous to the Néel's approximation used to describe magnetism of antiferromagnetic materials [91].

Following Equations 5.2-5.3, the effective fields h_a and h_b responsible for switching within sub-lattices A and B respectively, can be defined as

$$h_a = H - J'M_b \quad \text{and} \quad h_b = H - J'M_a, \tag{5.5}$$

where $J' = JN/2$. In the following we drop the prime and denote the interaction strength simply by J. The average states M_a and M_b in Equation 5.5 can then be expressed as:

$$M_a = \frac{2}{N}\sum_{i\in A} s_i^A(H - JM_b) = \hat{P}[H - JM_b] = \hat{P}[h_a], \tag{5.6}$$

$$M_b = \frac{2}{N}\sum_{i\in B} s_i^B(H - JM_a) = \hat{P}[H - JM_a] = \hat{P}[h_b], \tag{5.7}$$

with $N/2$ being the number of spins within a sub-lattice, and $\hat{P}$ the Preisach hysteresis operator. Thus, the Néel's type mean-field RCIS model (NMF) is one where

two identical Preisach hysteresis operators are coupled to each other. The coupling constant $J > 0$ corresponds to the strength of the antiferromagnetic interaction.

5.3.1 RPM in the Néel's mean field model (NMF)

Consider the single spin flip dynamics limit defined in Section 4.4. Assuming that the external field H increases starting from the negative saturation, the dependences of the sub-lattice magnetizations M_a and M_b on H can be expressed via the following coupled integral equations:

$$M_a = -1 + 2 \int_{-\infty}^{-JM_b+H} \rho(\alpha)\, d\alpha, \tag{5.8}$$

$$M_b = -1 + 2 \int_{-\infty}^{-JM_a+H} \rho(\alpha)\, d\alpha, \tag{5.9}$$

where $\rho(\alpha)$ is a spin threshold probability distribution. We assumed that the number of spins in each sub-lattice is sufficiently large, such that $\rho(\alpha)$ can be viewed as a smooth function, and hence we can replace the summations in Equations 5.6-5.7 by an integration. Subtracting the second equation from the first and changing the variables to $M = (M_a + M_b)/2$ and $\psi = (M_a - M_b)/2$, gives after arrangement the relation:

$$\psi = \int_{-J\psi}^{+J\psi} \rho(\alpha - JM + H)\, d\alpha. \tag{5.10}$$

After substituting $\alpha \to J\psi\alpha$, the above expression reduces to:

$$\psi = J\psi \int_{-1}^{+1} \rho(J\psi\alpha - JM + H)\, d\alpha, \tag{5.11}$$

or equivalently:

$$\psi \left(1 - J \int_{-1}^{+1} \rho(J\psi\alpha - JM + H)\, d\alpha \right) = 0. \tag{5.12}$$

Since $\rho(x)$ is the probability distribution, and thus $\rho \geq 0$ for every x, the following inequality certainly holds:

$$0 \leq \int_{-1}^{+1} \rho(x)\, dx \leq \int_{-1}^{+1} \rho_{\max}\, dx = 2\rho_{\max}, \tag{5.13}$$

where $\rho_{\max}$ is the maximum of the probability distribution ρ. Therefore, if $2J\rho_{\max} \leq 1$, Equation 5.12 will have only a trivial solution $\psi = 0$ (which implies $M_a = M_b$). Nontrivial solutions $\psi \neq 0$ ($M_a \neq M_b$) are technically possible if $2J\rho_{\max} \geq 1$. Hence, the critical interaction at which qualitatively new solutions appear equals to:

$$J_c = \frac{1}{\rho_{\max}}. \tag{5.14}$$

We now show that RPM holds for $J < J_c$. The argument can be divided into three steps: 1) If $\psi = M_a - M_b = 0$, then the local fields $h_a = h_b = h$ and Equations 5.6-5.7 can be rewritten as:

$$M_a = M_b = \hat{P}[h]. \tag{5.15}$$

Since the Preisach operator $\hat{P}$ has the RPM property, closed cycles of h must result in closed cycles of both M_a and M_b. Moreover, the operator relation given by Equation 5.15 is invertible because the threshold distribution ρ is smooth and non-negative and the inverse $\hat{P}^{-1}$ is also a Preisach operator [57, 92]. As a result, the relations $h = \hat{P}^{-1}[M_a]$ and $h = \hat{P}^{-1}[M_b]$ also have RPM property, i.e. closed magnetization cycles must produce closed h-cycles. 2) Using Equation 5.5, the relationship between H and h can be written as

$$H = J\hat{P}[h] + h = \hat{N}[h], \tag{5.16}$$

where $\hat{N}[h]$ is again a Preisach operator, since the first term in Equation 5.16 is a Preisach operator and the addition of a linear term h just tilts the hysteresis loops. Hence, the relationship given by Equation 5.16 has to have the RPM, as well as the inverse. 3) Using the fact that relations defined by Equations 5.15-5.16 and their inverses have the RPM, the relations $M_a(H) = M_b(H)$ must also have RPM. This proves the existence of closed cycles for interactions J below the critical strength J_c.

5.3.2 Cycle opening in the NMF

As shown in the previous section, nontrivial solutions of Equation 5.12 are possible if $J > J_c$. To see that such solutions exist, we solve Equation 5.12 numerically assuming a Gaussian distribution of thresholds $\rho(\alpha)$. Note that given the relation defined by Equation 5.14, the critical interaction J_c can be related to the variance σ of the Gaussian distribution simply as $J_c = \sigma\sqrt{\pi/2}$. The critical interaction is therefore directly determined by the disorder level present in the system.

Dependence of $\psi = M_a - M_b$ on the field point H along the increasing branch of the hysteresis loop $M(H)$ is plotted in Figure 5.3. Different interaction magnitudes below and above the J_c are considered. Figure shows that the difference ψ is zero for $J < J_c$, becoming nonzero for $J > J_c$ and growing as the interaction strength increases. In addition, as shown in the inset in Figure 5.3, the emergence of the nonzero difference ψ is also manifested as a bending of the major loop branch around to coercivity, i.e. by macroscopically observable changes of hysteresis behavior.

While we found no analytical way to show that the RPM is not preserved for $J > J_c$, numerical simulations confirm abrupt onset of the cycle opening. In these numerical simulations we assumed only continuous threshold distribution functions $\rho(\alpha)$, which is equivalent to using an infinitely large set of bistable switches. The trade-off is that a number of iterations needed to find stable states of the mean-field

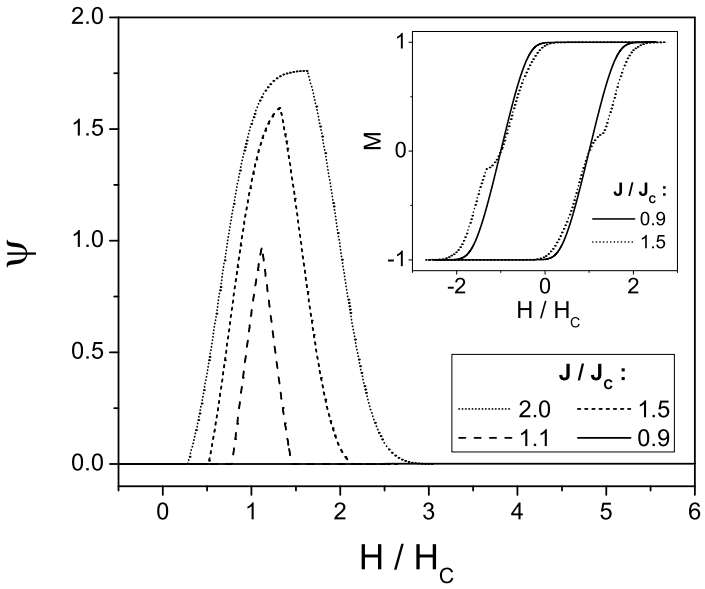

Figure 5.3: Difference $\psi = M_a - M_b$ versus the external field H along the increasing major hysteresis loop branch (H_c is the coercive field where $M = 0$). $\psi = 0$ for $J < J_c$ and $\psi \neq 0$ for $J > J_c$. The maximum difference appears around the coercive field. The results correspond to the Gaussian distribution of thresholds with variance $\sigma = 1$, when $J_c = (\pi/2)^{1/2}$. The inset shows a change of shape of major hysteresis loop for $J > J_c$ when $\psi \neq 0$.

model also becomes infinite and iterations need to be terminated when the relative change of magnetization becomes sufficiently small. In our simulations this number is 10^{-8}.

To investigate the onset of the cycle opening, we considered only minor cycles that are attached to the increasing branch of the major hysteresis loop. Starting from the negative saturation, the field H is increases until the point H_u when it is reversed down to H_d, then reversed again and increased back to H_u. The pair of variables (H_d, H_u) uniquely defines each minor cycle attached to the major hysteresis loop. The cycle opening ΔM will be measured as a difference in magnetizations before and after the cycle, i.e. as $\Delta M = M_1 - M_2$, and depends on both upper and

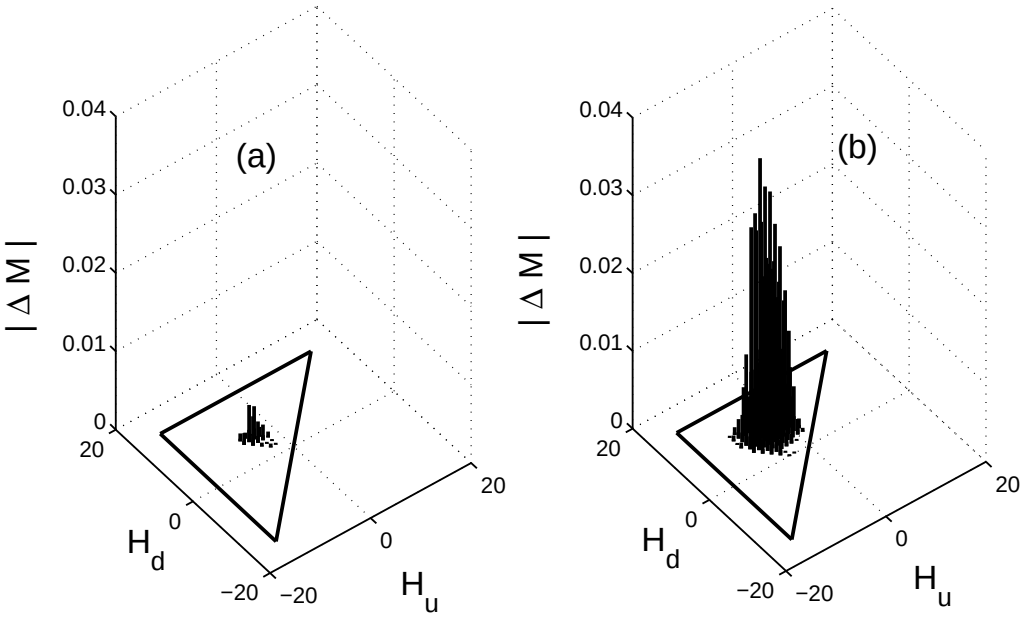

Figure 5.4: A sequence of cycle openings $|\Delta M|$ numerically calculated for Néel's mean-field RCIS with a Gaussian distribution of thresholds ($\sigma = 1$, $\mu = 4$). Interaction strengths are: a) $J = 1.04J_c$, b) $J = 1.2J_c$.

lower reversal fields. We will be interested in the magnitude of the cycle opening, $|\Delta M| = |M_1(H_u) - M_2(H_u)|$, obtained after the first external field period. An example of such a cycle opening function is shown in Figure 5.4, and has been obtained numerically by first meshing the (H_d, H_u) plane and then simulating the minor cycles for each discrete point on this mesh. As soon as the interaction strength J exceeds J_c, the open minor cycles appear in a small region of the reversal fields $H_u > H_d$ (Figure 5.4(a)). As the interaction strength increases, both the region of reversal fields corresponding to open cycles and the magnitude of the opening increase as well(Figure 5.4(b)).

Finally we note, that similar conclusions have been obtained also for e.g. Lorenzian, log-normal, and triangular threshold distributions $\rho(\alpha)$. In all cases, the observed loss of the RPM and the onset of the cycle opening was directly associated with the transition interaction J_c.

5.4 Summary

In this chapter we analyzed the origins of the cycle opening in the interaction networks. We showed that as long as the interactions are positive, minor cycles remain closed independently of the structure of interaction network. Similar general conclusion, however, cannot be made about networks with negative interactions. We gave two examples of antiferromagnetic networks where the loop closure holds, particularly the mean field and Néel's mean field RCIS models. In the Néel's mean field RCIS model, the RPM has been shown to hold for sufficiently small interactions. Cycle opening appeared suddenly at some critical interaction strength which has been shown to depend on the disorder level. Néel's mean field RCIS model is thus an example of a simple system, where both RPM and cycle opening can be observed, depending on the structural parameters. Based on the analysis in this chapter, we conclude that there are two necessary conditions for existence of open cycles: 1) negative interactions between the spins, and 2) more than one variable necessary for full description of the state of the system.

Chapter 6. Cycles in the RCIS with short range interactions

In Chapter 5 we demonstrated that the Néel's mean field model displays an abrupt appearance of open cycles at a certain transition interaction J_c. The value of J_c has been shown to be fundamentally linked to the disorder level present in the system. In this chapter, we depart from the mean field type modeling and investigate the behavior of cycles in the often more realistic RCIS model with short range interactions. The goal is to understand the origin of the cycle opening and its relation to the disorder level.

6.1 RCIS on a 2-dimensional lattice

Consider RCIS model with spins distributed on a two-dimensional lattice and assume interactions only between the immediately neighboring spins. Once again, we consider the single spin flip dynamics introduced in Section 4.4. Assuming a Gaussian distribution of thresholds with $\mu >> \sigma$, the upper bound on the interaction strength can be found from Equation 4.7 and equals $J < J_t = (\mu - 3\sigma)/4$, where we used the fact that each spin on the lattice has 4 neighbors and thus $d_{\max} = 4$.

We performed numerical simulations to study the behavior of minor cycles. Cycle opening functions $|\Delta M| = |M_1(H_u) - M_2(H_u)|$, where M_1 and M_2 are respectively the magnetization values before and after the minor cycle excursion, were calculated for different interaction strengths J. Two measures were defined to characterize the cycle opening: 1) the extent of the opening region Ω_o, equal to the area of that region in the reversal-field-plane (H_u, H_d) which corresponds to open cycles, and 2) the

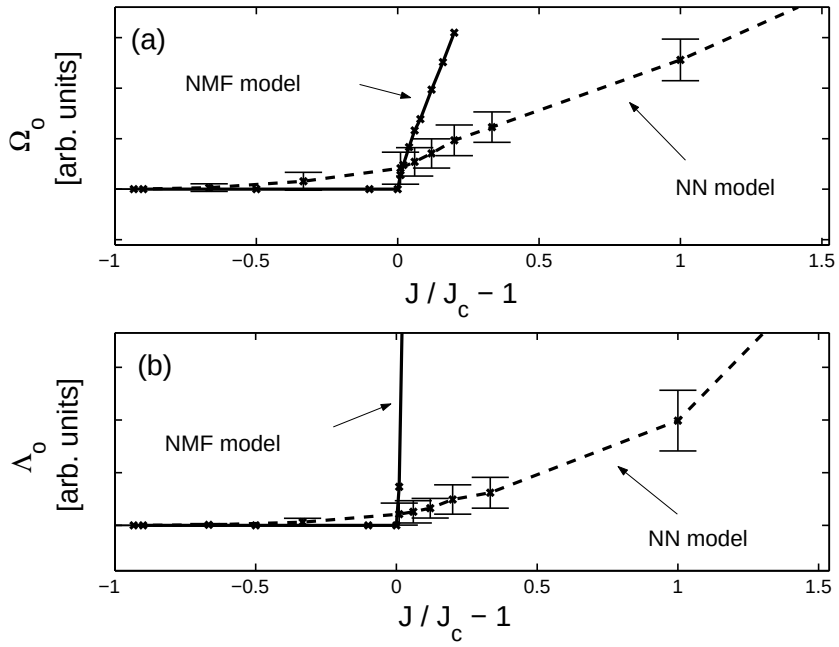

Figure 6.1: The opening region Ω_o (top) and the extent of the cycle opening Λ_o (bottom) as a function of normalized interaction strength for, respectively, the 2D nearest neighbor RCIS and the Néel's mean field RCIS models. The system size considered was 1600 spins and the data for the nearest neighbor model was averaged over 20 different random threshold realizations (Gaussian distribution with variance $\sigma = 1$, mean $\mu = 4$).

extent of cycle opening defined as an integral over the Ω_o, i.e.:

$$\Lambda_o = \int_{\Omega_o} |\Delta M| \, dH_d dH_u. \tag{6.1}$$

Thus, while Ω_o corresponds simply to the number of open minor cycles attached to the ascending branch of the major hysteresis loop, the function Λ_o carries also information about the average opening of those minor cycles.

Figure 6.1 shows a comparison of minor cycle behavior for the nearest neighbor RCIS model (dashed line) and for the Néel's mean field RCIS model (solid line), which has been developed in Section 5.3. The top part of figure shows a dependence of the cycle opening range Ω_o on the interaction strength, while the bottom part of

figure shows the interaction dependence of the extent of loop opening Λ_o. A threshold variance $\sigma = 1$ was assumed for both models. In addition, data obtained from the nearest neighbor model (NN) has been averaged over 20 realization of randomness. Note the normalization of the interaction magnitude J by the critical point J_c. In the case of the Néel's mean field model (NMF), the value of $J_c = 1.253$ has been obtained simply by using Equation 5.14. Determination of J_c is complicated in the case of the NN model, where an abrupt onset of open cycles has not been observed. We have therefore determined the value of J_c as an average over the number of minimum interaction strengths, obtained for each realization of disorder randomness, at which the open cycles could be seen first. For the data shown in Figure 6.1, we found $J_c = 0.15 \pm 0.01$. Note also, that for $J > J_c$ the quantities Ω_o and Λ_o grow very rapidly in the case of the NMF model while their growth is slower in the case of the NN model.

The question arises if the emergence of open loops could be associated with an out of equilibrium phase transition occurring as the interaction and disorder parameters are tuned. If yes, could the NMF model discussed in the previous chapter be viewed as a mean field approximation to NN with regard to such phase transition behavior? First of all, as we find here, the NMF model yields very different critical interaction strength J_c than the NN model. This is, however, not entirely unexpected. In fact, it is well known that mean field models often do not predict the critical behavior accurately. For example, it is found in the study of the RFIM that its mean-field approximation does not predict the critical disorder correctly [69]. Also the mean-field models used in the equilibrium thermodynamics typically do not predict the critical points and critical exponents accurately in many low dimensional systems [93]. Secondly, as seen from the plots in Figure 6.1, we actually do not observe abrupt onset of the cycle opening in the case of the NN model. There could be several reasons for the absence of a sharp transition in the NN models: 1) Finite size effects due to the

insufficient number of spins used in the modeling. Although we considered lattices of up to 10^6 spins, further increase of the system size might be, and seems to be necessary. 2) The dimension 2 of the lattice could be smaller than the lower critical dimension for the existence of phase transition in the model and strong fluctuations of the order parameter destroy any long range ordering. In such case, the phase transition cannot be observed at all. To address this issue, we have also considered model with spins on a three dimensional lattice. However, such studies did not yield convincing results either, and moreover, the analysis of higher dimensional systems is more complicated due to more pronounced finite size effects. 3) It is possible, that we do not deal with any critical phenomena in case of NN model. This possibility is investigated in the next section.

6.2 Ensemble of spin triplets

To eliminate the effect of correlations and thus the possibility of any phase transition behavior, we divide the lattice into independent spin triplets. Spin triplets are the smallest networks producing open cycles (ensemble of spin couples produces always closed minor cycles).

6.2.1 Definition

Consider a group of P 5-spin chains where the nearest neighbors interact via anti-ferromagnetic interaction $-J$, $J > 0$. Assume that the boundary spins are fixed in either $+1$ or -1 state depending on the random choice (Figure 6.2). Thus there are only three spins in each chain which can flip as the external field changes. Let these variable spins in any k-th triplet be denoted as s_1, s_2, s_3, and their thresholds as α_1, α_2, α_3. We assume that all thresholds in the ensemble are independent random variables given by probability distribution $\rho(\alpha)$. A single spin flip dynamical limit

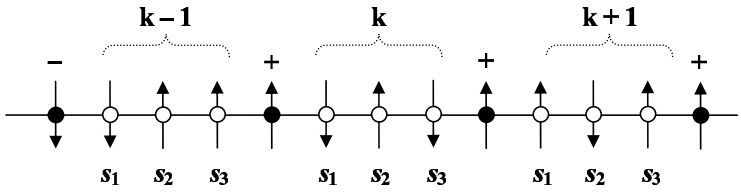

Figure 6.2: Definition of an ensemble of independent spin triplets. Every fourth spin (black) is frozen in a given state (chosen randomly to be either $+1$ or -1) specifying boundary conditions for the spin triplets. Hence, possible boundary conditions are $+/+$, $-/-$, $-/+$ and $+/-$.

will be assumed, which for a Gaussian threshold distribution with $\mu >> \sigma$ requires restriction $J < J_t = (\mu - 3\sigma)/2$ because the maximum number of neighbors of each spin is 2 and thus $d_{\max} = 2$ in Equation 4.7.

Since the $+1$ and -1 states of the boundary spins are chosen randomly, there are 4 possible combinations of boundary conditions, respectively $-/-$, $-/+$, $+/-$, $+/+$. Assuming every combination to be equally likely, for a large ensemble there will be $P/4$ spin chains with a particular set of boundary conditions. Then, since there are 6 different ways for ordering the thresholds among the spins s_1, s_2, s_3, there will be total 4×6 different spin triplets in the ensemble, such as e.g. $\alpha_1 < \alpha_2 < \alpha_3$ $(-/-)$ or $\alpha_2 < \alpha_1 < \alpha_3$ $(-/+)$ and so on. For a very large ensemble, there will be $P/24$ triplets of a particular type.

6.2.2 Origin of the cycle opening

Although there are 24 qualitatively different types of spin triplets, an extensive search through all possibilities reveals that only two types display open cycles. In particular, open cycles are produced by spin triplets with

$$T_a: \quad \alpha_2 < \alpha_1 < \alpha_3 \ \ (-/-), \tag{6.2}$$

$$T_b: \quad \alpha_2 < \alpha_3 < \alpha_1 \ \ (-/-), \tag{6.3}$$

if and only if the differences between any two thresholds are smaller then $2J$, i.e. if $|\alpha_i - \alpha_j| < 2J$. Since both cases are related by the reflection symmetry about the central spin, it is sufficient to analyze one of them. We will consider the triplet type T_a satisfying the Condition 6.2. Results for T_b can be obtained right away by interchanging the indices 1 and 3.

Switching diagram for the triplet T_a is shown in Figure 6.3. This diagram shows all possible inherent states of a triplet, as well as all switching transitions between these states. For example, if the field H increases from negative to positive saturation, the switching transitions occur at thresholds a, d and e before the positive saturation state is reached. On the other hand, the transition at the field b is possible only after first reversing the field at some value $H > e$, decreasing it to $E < H < D$, then reversing again and increasing it back towards b. This history of the reversal fields, with negative saturation as an initial state, will be denoted by the brackets $b[D, e]$. For example, a symbol $c[B, d]$ means that switching at the threshold c can occur after first switching up at d, then reversing the field and decreasing it until switching down occurs at the threshold B, reversing the field again and increasing it back towards the threshold c. The table on the right hand side in Figure 6.3 shows the actual values of the switching fields, given the magnitudes of spin thresholds and the interaction.

O_M opening type: Open cycles with $\Delta M \neq 0$. Having developed the terminology, cycle opening is now easily demonstrated following the switching diagram in Figure 6.3. Consider the dashed line first. Assume that starting from the negative saturation the external field H increases up until the reversal point at H_r, such that $e < H_r < f$. At this field, all spins in the triplet T_a are in the positive state. When H is reversed and decreases, the central spin is the first spin to flip down at the field A. If the field is reversed at H_d lying somewhere in the range $D < H_d < A$ and increased

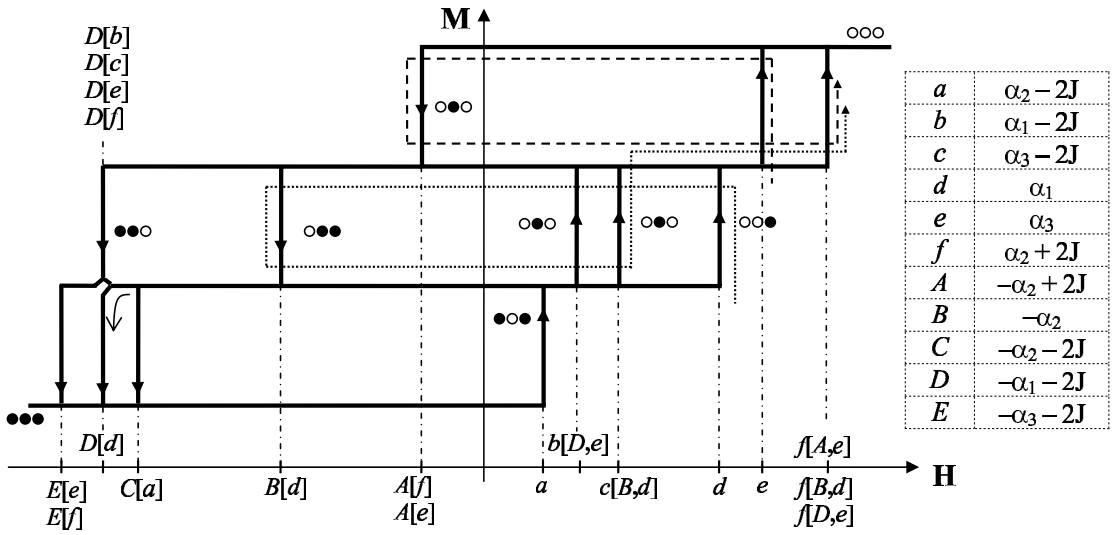

Figure 6.3: Complete switching diagram corresponding to the T_a-type triplet. Negative saturation is assumed as an initial state. Black (•) and white (∘) circles correspond respectively to negative and positive spins and represent the state of the triplet after the transition. Switching fields for spins flipping to positive (negative) state are denoted by lower case (capital) letters. The symbols in the brackets denote consecutive reversal fields required to obtain given switching. For example, $A[f]$ means that the flipping from the state $(\circ\,\circ\,\circ)$ to $(\circ\,\bullet\,\circ)$ accruing at the threshold field A requires previous field reversal at the point $H_r > f$. Dashed line shows cycle with reversal points $D < H_d < A$ and $e < H_r < f$, which does not return to the same state. Dotted line shows cycle with reversal points $D < H_d < B$ and $d < H_r < e$, which does return to the same magnetization but not to the same microstate. The table on the right lists the switching threshold fields given the thresholds α_i and interaction strength J.

back, the initial reversal field value H_r is no longer sufficient for flipping the central spin back to the original state. Note that such switching would only be possible if $H_r > f$. This results in an open cycle since the magnetizations at H_r before and after the cycle differ. Subsequent field cycles between reversals H_d and H_r yield no further switching and the minor cycle remains closed. Therefore, stable minor loops appear in this model at the second external field period. Finally we point out, that a similar situation occurs for cycles with reversals $e < H_r < f$ and $E < H_d < D$. On the other hand, the cycle opening is not observed if $H_r > f$.

O_S opening type: Open cycles with $\Delta M = 0$. As it turns out, there exists an additional mechanism leading to cycle opening which is not manifested as a magnetization difference. Consider the dotted line shown in Figure 6.3. Assuming the negative saturation as an initial state and reversal points $D < H_d < B$ and $d < H_r < e$, we note that the switching up after the cycle occurs at a different threshold $c < d$. Although the same magnetization state is obtained after the field returns to H_r, the microstate is different (before the cycle: s_1, $s_2 = -1$, $s_3 = +1$; after the cycle s_1, $s_3 = -1$, $s_2 = +1$). Hence, the return point memory does not hold. Further cycles between the reversal fields H_d and H_r yield no further changes.

Denoting the difference between the microstates before and after the cycle by ΔS, we conclude that $\Delta M = \Delta S \neq 0$ for O_M cycles, while $\Delta M = 0$ and $\Delta S \neq 0$ for O_S cycles. The origin of the cycle opening in both cases is due to the different switching order of spins during the increasing and decreasing external field variations. As a consequence, certain switching transitions existing during the increasing field are not available when the field returns after the decrease.

6.2.3 Symmetric reversal fields

Assume ensemble of P triplets. There will be roughly $P/24$ triples of the type T_a. According to previous discussion, opening at a reversal field H_r can be produced only by those T_a triplets which have their spin-thresholds arranged to satisfy the inequality $e < H_r < f$ at that field. As the reversal field H_r varies, the number of T_a triplets satisfying this condition changes depending on the threshold probability distribution $\rho(\alpha)$. For example, if the support of $\rho(\alpha)$ is restricted to some interval $(\alpha_{\min}, \alpha_{\max})$ such that $\alpha_{\min} > 0$, then for very low reversal fields most of the thresholds e will be greater then H_r and minor cycles will be closed. Similarly, for very high reversal fields, almost all triplets will have thresholds f below H_r and minor cycles will be closed

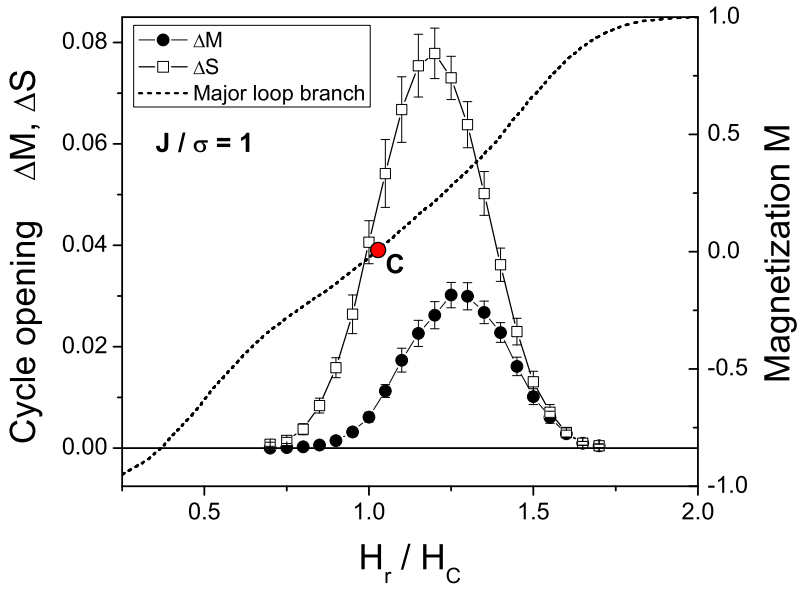

Figure 6.4: Differences in behaviors of the magnetization ΔM opening and the spin state ΔS opening for symmetric minor cycles with reversal points $H_d = -H_r$ (H_c is the major loop coercive field). The dashed line is the major hysteresis loop branch and the point C denotes its coercivity. Results have been obtained for an ensemble of 3000 triplets, Gaussian distribution of thresholds with variance $\sigma = 0.2$, and 10 realizations of randomness.

again. Thus, the magnitude of the reversal field H_r determines the relative number of triplets participating in the opening. The lower reversal field H_d is another variable determining the number of T_a triplets contributing to the opening at H_r. To be more specific, assume field cycles between symmetric reversal points $H_d = -H_r$ and $+H_r$. Let P_1 denote the number of triplets satisfying the condition $e < H_r < f$, and let P_2 denote the number of triplets satisfying the other condition $d < H_r < e$. Since according to Figure 6.3 it holds that $|A| < |B| < |e| < |D|$, there will be a fraction x_1P_1 of spin triplets from the group P_1 satisfying the inequality $D < -H_r < A$, and a fraction x_2P_2 of triplets from P_2 in the range $D < -H_r < B$. Notice, that x_1P_1 equals to the number of triplets producing O_M type opening and x_2P_2 are triplets producing

O_S opening. The sum $x_1P_1 + x_2P_2$ equals to the number of spin triplets producing total cycle opening of an ensemble at the symmetric reversal fields $H_d = -H_r$ and H_r.

Figure 6.4 shows a dependence of cycle openings ΔM and ΔS on the reversal field H_r for symmetric case with $H_d = -H_r$, obtained by simulating the ensemble of 3000 spin triplets with a Gaussian distribution of thresholds with $\sigma = 0.2$. The presence of both O_M and O_S mechanisms results in $\Delta M \neq \Delta S$. The dashed line in figure denotes an increasing major hysteresis loop branch showing that the effect is most pronounced after the coercivity, and disappears at low and large external fields. Note also, that $\Delta M \geq 0$ for every reversal point, which means that the magnetization after the cycle is always smaller then the magnetization value before the reversal. Such an effect is often observed in magnetism and has been referred to as negative tilting effect [12, 13].

6.2.4 Non-symmetric reversal fields

The question arises: Can the O_M and O_S mechanisms be separated by a suitable choice of reversal fields? The answer is yes, and as it turns out the O_S mechanism will be absent if $H_d \geq -H_r + 2J$. Only the O_M mechanism will be present in this case.

The argument is as follows. T_a triplets producing the O_S type opening at H_r must satisfy the conditions $d < H_r < e$ and $D < H_d < B$. According to Figure 6.3, the magnitudes of thresholds are $|d| = \alpha_1$, $|e| = \alpha_3$ and $|B| = |-\alpha_2| = \alpha_2$, and by the definition of T_a it must hold that $\alpha_1 - \alpha_2 < 2J$ and $\alpha_3 - \alpha_2 < 2J$. This means that $|d| - |B| < 2J$ and $|e| - |B| < 2J$. Hence, it is also true that $H_r - |B| < 2J$ which is equivalent to $B < -H_r + 2J$. Since $H_d < B$ is a necessary condition for the O_S type opening, it suffices to restrict $H_d \geq -H_r + 2J$ to guarantee absence of O_S cycles. It

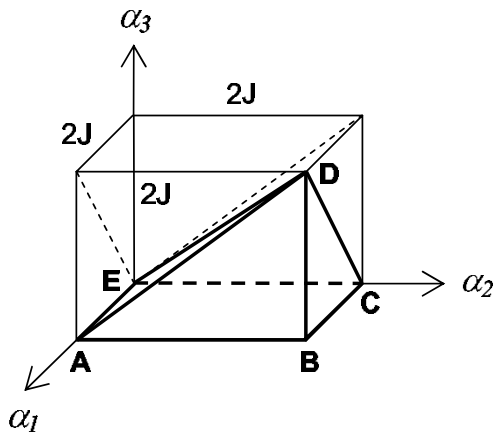

Figure 6.5: The O_M opening at the reversal field H_r is proportional to the volume of the pyramid ABCDE embedded in the cube having sides of the length $2J$ and being centered at the point $H_r - 2J$ in the α-space.

remains to check the possibility of O_M mechanism. Setting $H_d = -H_r + 2J$, it is easy to see that $|H_r - H_d| > |e - A|$. Therefore, any triplet T_a switching up at the threshold e can always switch down at the threshold A in the given range of reversals, and the O_M mechanism is possible. It can be shown, that O_M disappears for lower reversals $H_d \geq -H_r + 4J$ and all minor cycles then remain closed.

In the following we consider non-symmetric cycles with $H_d = -H_r + 2J$ and calculate the opening $\Delta M = \Delta S$ as a function of H_r. Since in this case O_M is the only mechanism responsible for the cycle opening of an ensemble, the problem reduces to calculating the number of T_a triplets (final result must be multiplied by 2 to include the identical case for T_b) having thresholds arranged to satisfy the inequality $e < H_r < f$ at the reversal H_r. Using the actual threshold values given in Figure 6.3, this inequality can be rewritten as $\alpha_3 < H_r < \alpha_2 + 2J$. Moreover, since according to Equations 6.2-6.3 it holds that $\alpha_2 < \alpha_1 < \alpha_3$, the thresholds of all three spins in the triplet T_a must satisfy the condition

$$H_r - 2J < \alpha_1,\ \alpha_2,\ \alpha_3 < H_r, \tag{6.4}$$

if that triplet is to produce the opening at H_r. Hence, to find the magnitude of the opening it is necessary to calculate the number of triplets satisfying simultaneously Conditions 6.2-6.3 and 6.4.

Since the thresholds are independent random variables, such calculation reduces to evaluating the volume of the pyramid ABCDE embedded inside the cube with a side length $2J$ and being centered at the point $H_r - 2J$ in the $\alpha_1\alpha_2\alpha_3$ parameter space (Figure 6.5). This calculation yields:

$$\Delta M = \Delta S = A \int_{H_r-2J}^{H_r} dt_1 \rho(t_1) \int_{H_r-2J}^{t_1} dt_2 \rho(t_2) \int_{H_r-2J}^{t_2} dt_3 \rho(t_3), \tag{6.5}$$

where the normalization constant $A = 1/3$ as shown below. Function ρ is the spin threshold probability distribution. The constant A is evaluated as follows. When the interaction J has a very large magnitude, such that the interval $(H_r - 2J, H_r)$ is much wider then the width of the threshold distribution ρ, there will certainly exist some reversal field value H_r at which all triplets from the groups T_a and T_b participate in the opening, i.e. total $N/36$ triplets from the entire ensemble (N is the total number of spins). Since each of these triples produces magnetization opening $2/N$ (spin up minus spin down) the maximum opening ΔM of the ensemble is:

$$\Delta M_{\max} = \frac{2}{N}\frac{N}{36} = \frac{1}{18} \approx 0.055. \tag{6.6}$$

To evaluate integral in Equation 6.5, we observe that if the interaction J is sufficiently large all thresholds will be contained within the cube shown in Figure 6.5, and the integral will be equal to 1/3 of the volume of this cube. Since the distribution function ρ is normalized to unity, the value of the integral for very large values of J approaches 1/3. Therefore, according to Equations 6.5-6.6, it holds that $\Delta M_{\max} = 1/18 = A/2/3$ and hence $A = 1/3$.

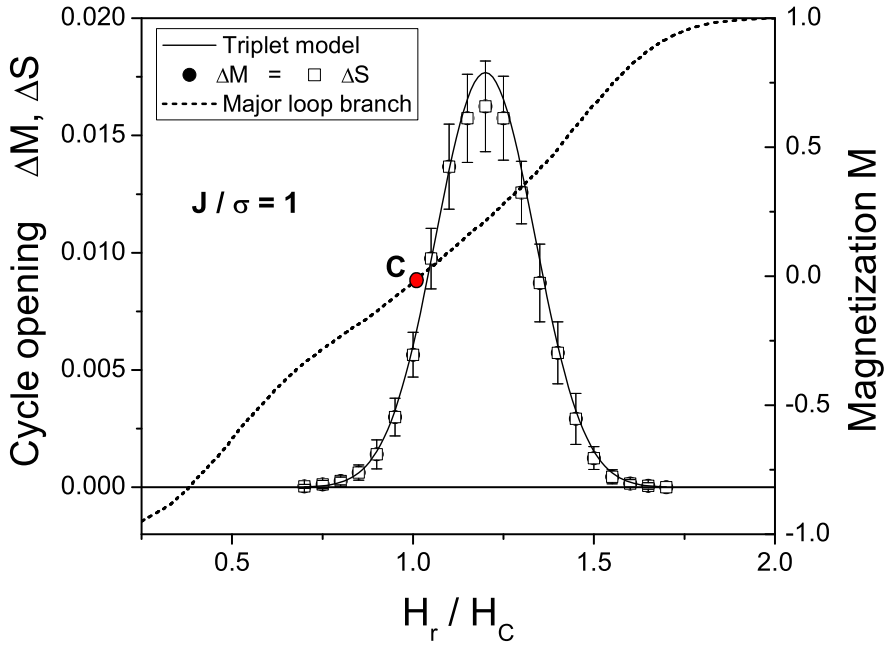

Figure 6.6: Cycle openings $\Delta M = \Delta S$ versus the reversal field H_r for non-symmetric minor cycles with reversal points $H_d = -H_r + 2J$ (H_c is the major loop coercive field). The dashed line is the major hysteresis loop branch and the C point denotes its coercivity. Results have been obtained for an ensemble of 3000 triplets, Gaussian distribution of thresholds with variance $\sigma = 0.2$, and 10 realizations of randomness.

The solid line in Figure 6.6 shows a dependence obtained from Equation 6.5, for $J \approx \sigma$ and a Gaussian distribution ρ of thresholds with variance $\sigma = 0.2$. Simulation data are added as points for comparison. The small deviations from the theoretical calculation around the peak are most likely due to the finite system size considered in simulations ($P = 3000$). The effect becomes significant only for reversal points around the coercivity, and diminishes as the field approaches positive saturation. Note also, that the simulated points for ΔM overlap with the points for ΔS, which confirms that only the O_M opening type exists for non-symmetric minor loops $H_d = -H_r + 2J$.

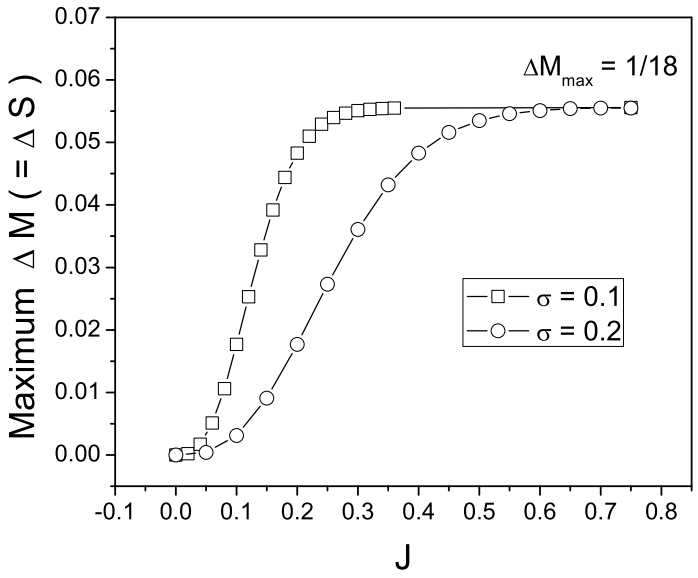

Figure 6.7: Dependence of the maximum opening $\Delta M = \Delta S$ on the interaction strength for two different disorder magnitudes. Results were obtained by using Equation 6.5, for Gaussian distribution ρ with mean $\mu >> \sigma$. The cycle opening saturates for $J >> \sigma$ reaching the universal constant 1/18, and the approach to saturation is faster (i.e. lower interactions are needed) for smaller disorder σ.

6.2.5 Cycle opening versus the interaction

Given the previous analysis and Equation 6.5 it is now clear that cycle opening at a given interaction strength depends on the probability of finding the triplets with specific arrangements of thresholds. As the interaction magnitude decreases, the length of the interval $(H_r - 2J, H_r)$ shrinks and the probability to satisfy Condition 6.4 by all three thresholds in the triplet decreases. The effect of the disorder is opposite; decreasing the variance of the threshold distribution increases the probability to find all thresholds in the interval $(H_r - 2J, H_r)$. In the limit $J/\sigma >> 1$, all T_a and T_b triplets will eventually satisfy Condition 6.4 and the effect saturates. This behavior is shown in Figure 6.7, displaying the maximum opening at a given interaction strength

for two different disorder levels. As shown, the saturation value $\Delta M_{\max} = 0.055$ given by Equation 6.6 is reached in both cases. This value is a universal constant of the model. The approach to saturation is faster for smaller disorder level.

Figure 6.7 is similar to Figure 6.1 in Section 6.1. There we considered the possibility of cycle opening taking place via the phenomena similar to phase transition. Analysis in this section suggests, however, that the cycle opening depends on the probability of specific threshold arrangements, and is not due to the long range correlation effects.

6.3 Summary

In this chapter we studied cycle opening in the RCIS model with short range interactions. As opposed to mean field models analyzed in the previous chapter, an abrupt appearance of open cycles is not observed. Open cycles exist for any interaction, and their occurrence probability, for a given disorder level, increases with the interaction magnitude. Then, to rule out any long range correlations effects possible for complicated interaction networks, we also considered an ensemble of independent spin triplets which is the simplest model yielding the cycle opening. We find that cycle opening in such a model depends only on the relative arrangement of thresholds in a particular type of triplets, and we derive dependence of the cycle opening on the reversal field value for a given interaction and disorder. Moreover, we pointed out that it is necessary to distinguish between the minor cycles with symmetric and non-symmetric reversal fields, and that to yield the complete information, the cycle opening must be generally measured by comparing the microstate differences before and after the cycle.

Chapter 7. Random interaction networks

In this chapter we investigate the effects of the interaction network structure on the behavior of hysteretic cycles. We consider the RCIS model with spins distributed on the classical random interaction network. Properties of such networks have been discussed in Section 3.3. Note that previously analyzed RCIS with non-interacting spins (Preisach model) and the mean field model, both having the RPM property, can be viewed as limiting cases of the classical random network. The RCIS with the nearest neighbor interactions, on the other hand, is analogous to networks with intermediate degree of connectivity, and as seen in the previous chapter, such model produces open cycles. It is therefore expected that a gradual increase of the network connectivity between the non-connected and the fully connected limits will result in a nontrivial minor cycle behavior, with transitions between the RPM and cycle opening. An example is illustrated in Figure 7.1 showing two hysteretic cycles obtained for a network having 1% percent of all possible interaction links, while the inset in the figure shows the RPM appearing after reducing the network connectivity to 0.1%.

As will also be shown in this chapter, the changes in the network connectivity do not only affect the rate at which hysteretic cycles converge to minor loops but can also result in the emergence of non-converging cycles, which do not form minor loops after arbitrarily large number of external field periods. Such behavior will be shown to be associated with the presence of specific topological elements in the network structure, particularly with the fully interconnected spin groups (cliques) of size equal or greater than 4.

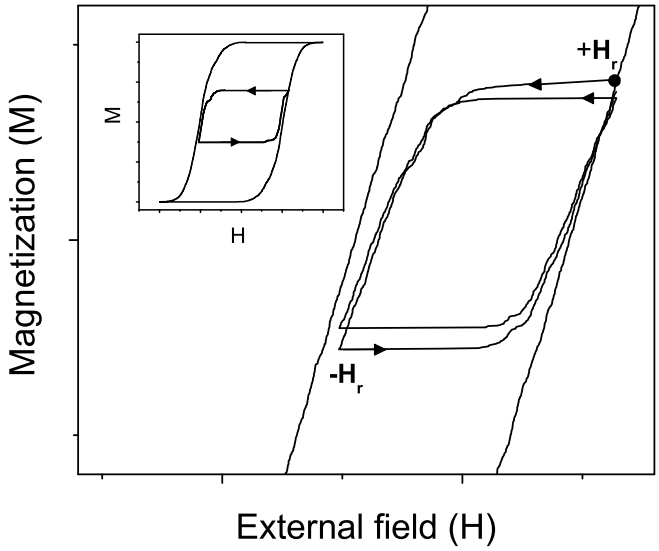

Figure 7.1: Two consecutive minor cycles with symmetric reversal fields $H_d = -H_r$ obtained using a random interaction network RCIS model with only 1% of all possible interaction links. Inset: Minor cycle closure observed after reducing the network connectivity to 0.1% of all possible interaction links.

7.1 Assumptions on the random RCIS networks

We consider classical Erdös-Rényi (ER) random network described in detail in Section 3.3.1. Such networks are considered to be the simplest realization of complex networks. Their connectivity and topological structure can be tuned by adjusting a single parameter: probability p of a connection between pairs of spins or by specifying the fraction n of the total $N(N-1)/2$ edges present. As discussed in Section 3.3.1 both choices are equivalent for large networks, where the connection probability can be related to the number of edges simply as: $p = 2nN^{-2}$. In our simulations, we generated random networks by specifying the number of edges, n, which where then randomly distributed among the N nodes using uniform random number generator. We consider negative (antiferromagnetic) interactions and the single spin flip dynam-

ics defined in Section 4.4. For a Gaussian distribution of thresholds with $\mu >> \sigma$, this assumption restricts the interaction magnitude range to $J < J_t = (\mu - 3\sigma)/d_{\max}$, where $d_{\max}$ is the maximum degree present in the network.

The number of interconnection links n in the network determines the interaction energy per spin. According to Equation 4.3 the spin-spin interaction energy of the antiferromagnetic system equals:

$$G_{s-s} = +J \sum_{ij} A_{ij} s_i s_j, \tag{7.1}$$

where $J > 0$. The average energy per spin, Δ, can be expresses as

$$\Delta = \left\langle -\frac{\delta G_{s-s}}{\delta s_i} \right\rangle = \left\langle J \sum_j A_{ij} s_j \right\rangle \approx J \cdot \left\langle \sum_j A_{ij} \right\rangle \cdot \left\langle s_j \right\rangle = J \cdot d \cdot M_r, \tag{7.2}$$

where d is the average network degree and M_r is the magnetization at the upper reversal point corresponding to field $+H_r$. In the following study, we will compare networks having different average degree d (i.e. different connectivity) for the same average energy per spin Δ. This amounts to adjusting the interaction magnitude $J < J_t$ using Equation 7.2 for every set of values Δ, d and M_r. Only cycles with symmetric reversal points $H_d = -H_r$ will be considered. The cycle opening will be quantified by the spin state difference ΔS, obtained by comparing the spin patterns before and after the cycle and calculating the %-difference of a number of spins that did not return to the original state. As discussed in the previous Chapter 6, ΔS is more robust measure than ΔM.

7.2 The first cycle opening versus the network connectivity

First, we study dependence of the first cycle opening ΔS on the average network degree d. We consider only symmetric minor cycles with the upper reversal H_r corre-

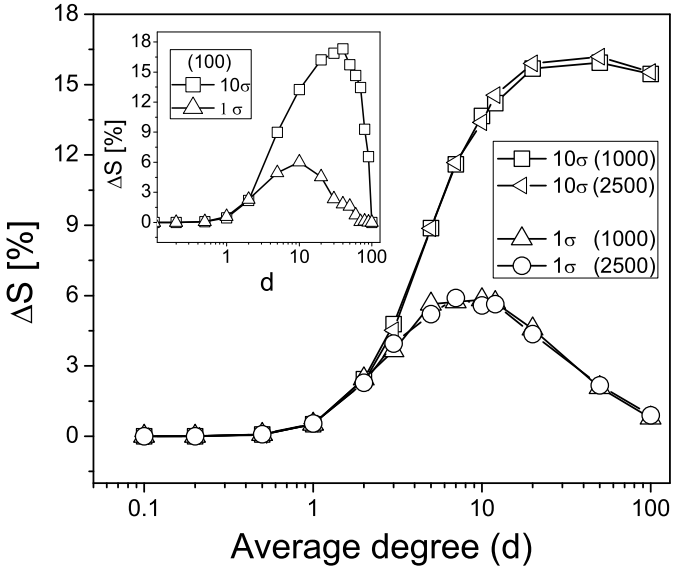

Figure 7.2: Percent difference ΔS between the microstates before and after the first minor cycle plotted for different degrees d of the interaction network. Only symmetric reversals with $H_d = -H_r$ are assumed, and H_r corresponding to the magnetization $M_r = 0.2$, where the effect is the strongest. Results are plotted for two system sizes $N = 10^3$ and 50^2 and the interaction energies $\Delta = 1\sigma$ and $\Delta = 10\sigma$ (σ is the variance of the Gaussian threshold distribution). Error-bars are about 1%. Inset: ΔS versus d for $N = 100$ showing that $\Delta S = 0$ for $d = N$. Error bars are about 4%.

sponding to magnetization $M_r = 0.2$. At this magnetization value, the cycle opening seemed to be most significant. Dependence of the cycle opening ΔS on the degree d obtained from simulations is shown in Figure 7.2 for two network sizes $N = 10^2$ and 50^2. As expected, $\Delta S = 0$ for $d << 1$, independently of the Δ/σ ratio, since the majority of spins are isolated or form couples. As discussed previously such antiferromagnetic systems have the RPM property (Section 5.2). The structure of the random network changes as d increases. When trees of order 3 and higher emerge (at $d \approx N^{-1/2}$, see Figure 3.5 in Section 3.3.2) the cycle opening becomes nonzero, although a well pronounced increase of ΔS is observed only after the percolation threshold of the ER network at $d \approx 1$. At this percolation threshold a giant spin

cluster appears in the network structure, and almost all nodes become connected (Section 3.3.2). As the connectivity of the network increases further, ΔS reaches maximum and then starts to decrease to zero as d approaches the network size N. In the mean field (fully connected network) limit $d \to N$, the RPM property is recovered and $\Delta S = 0$ as expected. Due to the computational expense, full numerical confirmation of this behavior has been possible only for a smaller system size $N = 100$ and is shown in the inset in Figure 7.2.

Numerical tests for different network sizes N (up to 50^2), different disorder σ and different average energy per spin Δ revealed that cycle opening ΔS depends on the ratio Δ/σ rather than on Δ and σ separately. We found no dependence on the mean μ of the threshold distribution in the assumed limit $\mu >> \sigma$. In addition, ΔS is observed to be independent of the network size as long as $d << N$, as demonstrated in Figure 7.2 by plotting the dependences for $N = 10^3$ or 50^2 in the degree range $d \leq 100 << N$. These results demonstrate that the first cycle opening ΔS does not depend on the topological properties of the network because the probability of finding various topological interconnection structures in the ER network, such as trees and cliques (completely interconnected sub-graphs), depends both on d and N. We note that this conclusion is supported also by other results not presented here, which have been obtained for a RCIS model on a regular 2D lattice with ΔS calculated as a function of the interaction range (which is, of course, proportional to the coordination number d).

7.3 Emergence of non-converging cycles

As shown above, the cycle opening depends on the average number of bonds linking the spins and not on the particular way the spins are interconnected, i.e. on the topological properties of the interaction network. However, as demonstrated in the

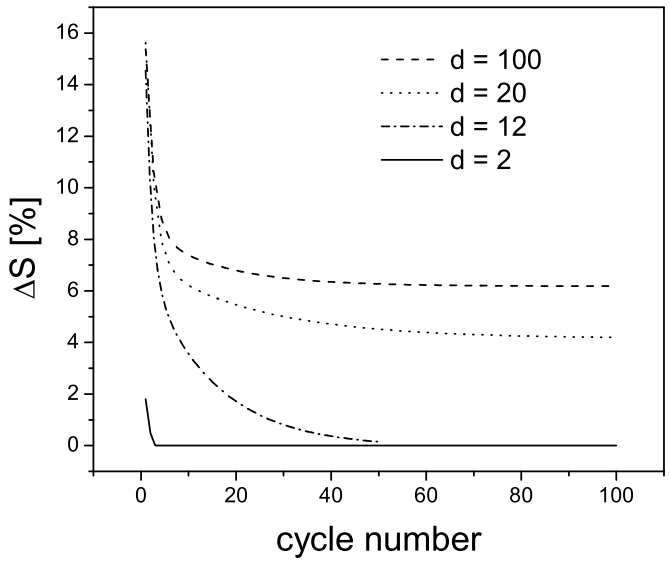

Figure 7.3: Dependence of the opening ΔS on the cycle number for different network degrees. For $d = 2$ and for $d = 12$ cycles converge within 4 and 50 cycles respectively. For $d > 13$ the cycle convergence becomes very slow as shown here for $d = 20$ and 100. The data is for 50^2 spin network and averaged over 50 random graph and disorder realizations. Error-bar level is about 1%. Data correspond to reversal magnetization $M_r = 0.2$, $\Delta/\sigma = 10$, and $\sigma = 0.1$.

following sections, the network topology plays a crucial role in determining the minor cycle convergence, i.e. the rate at which open cycles form minor loops.

To investigate convergence rates, we calculated the cycle opening ΔS by comparing the spin patterns before and after each consecutive cycle. As shown in Figure 7.3, the rate at which ΔS approaches zero depends on the network degree d. For $d = 2$, the network structure is dominated by trees and quickly stabilizing minor cycles are observed. Convergence rates decrease as the network degree d increases (e.g. dash-dotted line for $d = 12$). For $d > 13$, the behavior changes qualitatively and ΔS no longer converges to zero (although cycles are eventually expected to repeat due to the finite size of the networks being simulated). This is demonstrated in Figure 7.3 by dependences for $d = 20$ and 100.

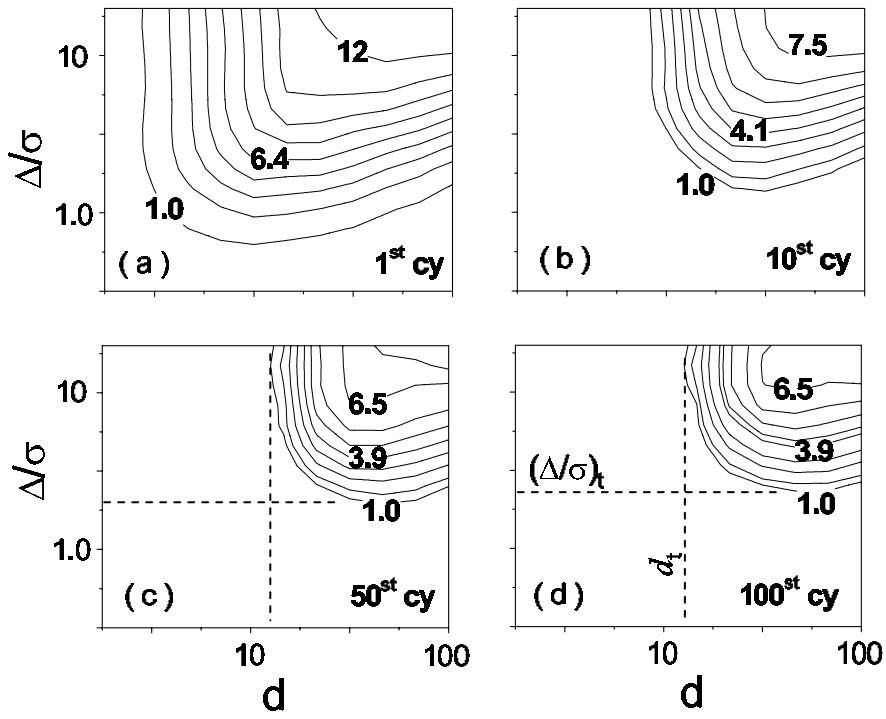

Figure 7.4: Contour maps showing the cycle opening ΔS for different values of the interaction energy Δ/σ and the network degree d (note the logarithmic scale of Δ/σ and d axes) for respectively: (a) 1-st, (b) 10-th, (c) 50-th, and (d) 100-th cycle. The lower bounds for the 'limiting' region with non-converging cycles correspond to $(\Delta/\sigma)_t = 2.3$ and $d_t \approx 13$. Data are for $N = 50^2$, $\sigma = 0.1$ and averaged over 50 random graph and disorder realizations. Error bars level is about 1%.

To confirm the existence of non-convergent cycles, we calculated ΔS versus the cycle number dependences for different Δ/σ ratio, connectivity parameter d and for different networks sizes N. An example of the $\Delta S(\Delta/\sigma, d)$ function is given by the contour plots in Figure 7.4(a-d) for four subsequent field cycle numbers and a fixed network size $N = 50^2$. It is illustrated that in the low $(\Delta/\sigma, d)$-parameter region closed minor loops with $\Delta S = 0$ appear already after a few initial field cycles (compare Figures 7.4(a-b)). The behavior in this region in the parameter space is analogous to the familiar tilting effect [12, 13]. More and more cycles seem to be required for the minor loop formation for higher Δ/σ and d values (Figure 7.4(c)). However,

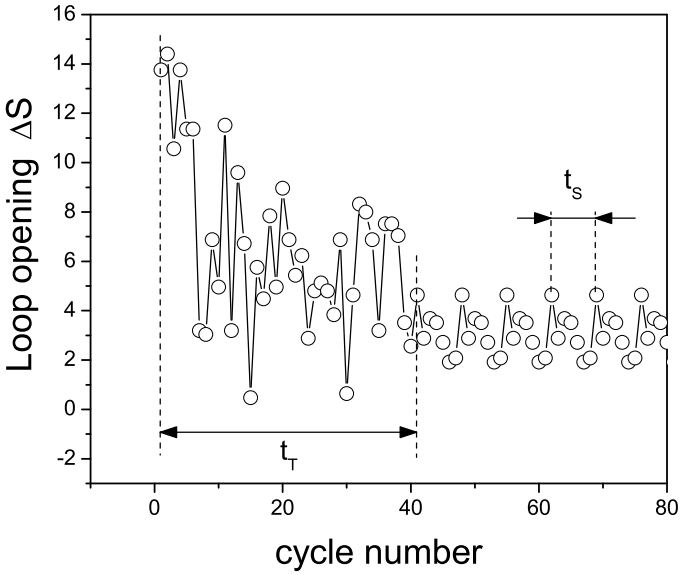

Figure 7.5: Definition of the transient t_T time and the subharmonic period t_S. The steady state cycles reached after initial transient time $t_T \geq 1$ can contain simple minor loops with $t_S = 1$ or subharmonic cycles with $t_S > 1$. Plot has been obtained for network with $d = 20$ and $N = 10^3$.

for the parameter region bounded from below by certain critical values $(\Delta/\sigma)_t$ and d_t (Figure 7.4(d)), closed minor loops often do not form even after 100 field periods. This region corresponds to non-convergent behavior shown in Figure 7.3. Quite surprisingly, we find that the value d_t is remarkably close to the theoretical value, $d_t = N^{1/3}$, at which the ER network is known to undergo a topological transition associated with the emergence of cliques of size 4 (fully interconnected groups of 4 spins; see Section 3.3.2). This issue will be discussed further in Section 7.4.

7.3.1 Two different types of non-converging cycles

Since the results shown in Figures 7.3 and 7.4 were averaged over 50 different random network and disorder realizations, it is possible that certain information about

the nature of non-converging cycles might have been lost during the averaging procedure. Analyzing each network realization separately indeed reveals two different non-converging behaviors of cycles. An example is shown in Figure 7.5. After several initial cycles, defining the transient time t_T, the cyclic behavior settles to the steady state where the microstate repeats after a certain period number $t_S > 1$. In other words, the same microstate is recovered with a t_S multiple of the external field period, and obviously $\Delta S \neq 0$ after the arbitrarily large number of external field periods. Such S-type cycles (Figure 2.3(d)) have been observed previously for some spin glass networks and have been referred to as subharmonic cycles [37]. In addition to subharmonic loops, there exists non-converging cyclic behavior of different nature, particularly, cycles with a very long transient period $t_T > 100$. Presence of such cycles with very long transient time is a new and surprising observation and will be subject of our investigation in the following sections. Finally we note that both types of non-convergent cycles appear only for certain random network realizations, and frequency of their occurrence increases with the connectivity of the network.

7.3.2 Magnetization versus the spin state opening

We studied cycle opening not only by the ΔS measure, which is based on comparing the microstates before and after the cycle, but also by the ΔM measure based on the magnetizations. Dependences ΔM versus the cycle number for different network degrees are shown in Figure 7.6. Figure 7.6(a) for low connectivity network $d = 2$ shows genuine tilting effect. As d increases, fluctuations of ΔM emerge for both converging and non-converging cycles (Figures 7.6(b-c)). The apparent randomness in the ΔM variation results from the fact that, when the network degree d is large, there exist many different spin states having similar magnetizations (i.e. average states).

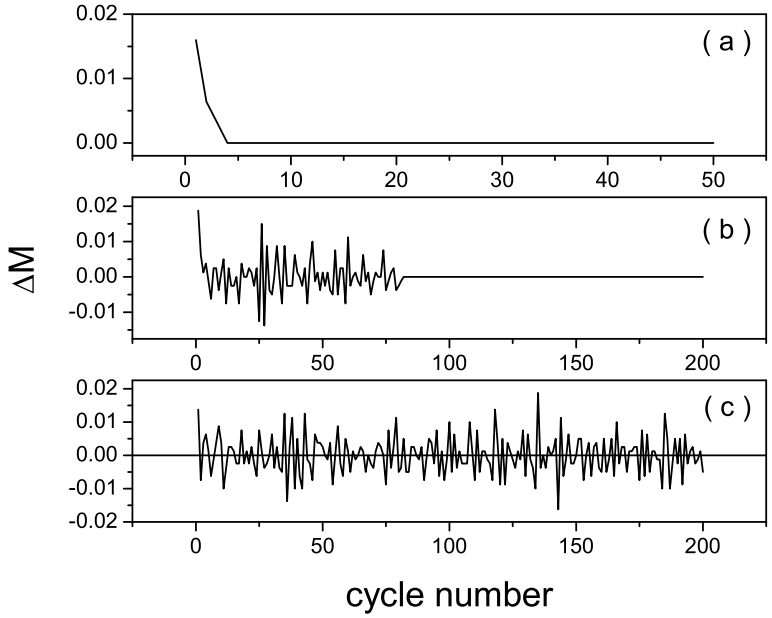

Figure 7.6: Dependence of the magnetization opening ΔM on the external field cycle number for different degrees. (a) Genuine tilting effect for low network connectivity $d = 2$, (b-c) Magnetization fluctuations for $d = 12$ and $d = 20$.

The fact that the ΔM based measurements of minor cycles often yield fluctuating (and thus inconclusive) results is well known from magnetism [7]. While it is in principle possible to record and compare microscopic magnetic patterns after each cycle rather than magnetization, such measurements are nontrivial [4–6]. Another possibility could be to relate statistics of the ΔM noise to the interaction structure of complex networks. Such investigations will be a subject of our future studies.

7.4 Diverging cycle length and the network structure

Two questions must be answered to confirm the existence of cyclic trajectories with diverging transient length t_T. In particular, as the network size N increases, 1) is the rate of increase of t_T faster than the rate of increase of N and 2) is the rate of

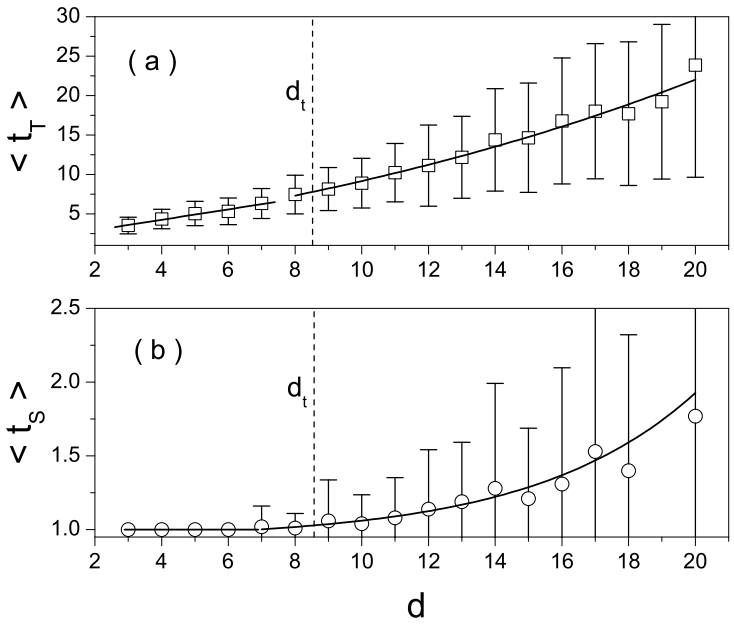

Figure 7.7: Dependence of the transient (a) and subharmonic (b) periods on the network degree. The vertical dashed line marks the theoretical value for the transition degree d_t at which first 4-cliques emerge. The data is plotted for a network size $N = 25^2$, when $d_t = N^{1/3} \approx 8.55$. (a) The $\langle t_T \rangle$ versus d data for $d < 8$ are best fitted by a linear function, while the exponential fit is better for $d > 8$. (b) Subharmonic cycles do not exist for $d < 8$ (then $\langle t_S \rangle = 1$). $\langle t_S \rangle$ vs. d data for $d > 8$ has been fitted by an exponential function. Symbol $\langle\rangle$ indicates, that data in the figures (a) and (b) is averages over 100 random network realizations. Data corresponds to reversal magnetization $M_r = 0.2$, $\Delta/\sigma = 10$, and $\sigma = 0.1$.

increase of t_S slower than N? The second condition is required to guarantee that the diverging cycles are not subharmonic cycles with very long period. The first condition guarantees the existence of non-converging cycles in the thermodynamic limit $N \to \infty$. The goal, therefore, is to compare cyclic behavior of networks of different sizes N.

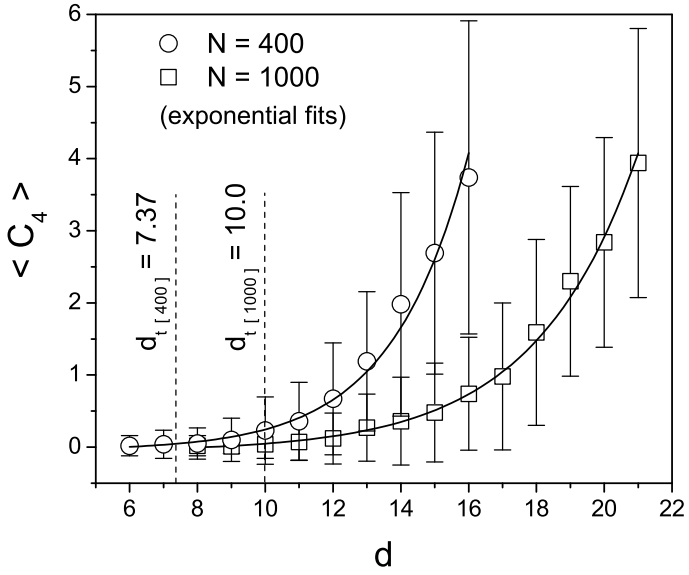

Figure 7.8: Dependence of the average number of cliques of size 4 on the network degree obtained for two different system sizes. Theoretical values for appearances of 4-cliques are $d_t = 7.37$ for $N = 20^2$ and $d_t = 10$ for $N = 10^3$. As shown, for finite size nets the 4-cliques appear at $d < d_t$. Averages have been calculated over 100 random network realizations. Data corresponds to reversal magnetization $M_r = 0.2$, $\Delta/\sigma = 10$, and $\sigma = 0.1$.

7.4.1 How to compare cycles for networks of different size?

Based on the results obtained in Section 7.3, we hypothesized that the appearance of non-converging cycles could be associated with presence of the 4-th order complete subgraphs (cliques) in the network structure. For infinite networks, such topological elements are expected to emerge at the transition degree $d_t \approx N^{1/3}$ (note that d_t is expected to be reduced for finite size networks). Indeed, as indicated in Figures 7.7(a-b), showing dependences t_T vs. d and t_S vs. d obtained for the network size $N = 625$, there are changes in the trends closely below the theoretical degree d_t (dashed vertical line). Since the degree is tuned smoothly and the only change in the network structure in the plotted range of degrees d is the emergence 4-cliques, these changes in the trends

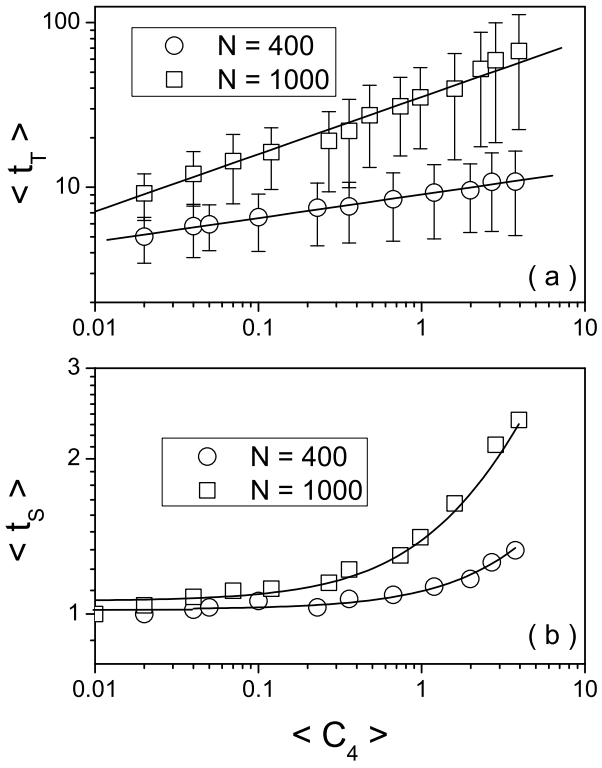

Figure 7.9: (a) Power law dependence of the average transient length on the density of 4-cliques. (b) Dependence of the average subharmonic length on the density of 4-cliques. The network sizes considered are $N = 20^2$ and 10^3, and the averages $\langle t_T \rangle$, $\langle t_S \rangle$ and $\langle C_4 \rangle$ are calculated over 100 network realizations. Data corresponds to reversal magnetization $M_r = 0.2$, $\Delta/\sigma = 10$, and $\sigma = 0.14$.

must be associated with these topological structures. However, the value $d_t = N^{1/3}$ is exact only for infinite size networks $N \to \infty$ and can differ for finite networks. To find the actual value of d_t for our networks, we performed a search through every random network realization and counted the number of 4-cliques present. This number of 4-cliques for a given random network realization will be denoted as C_4. The dependence of an average $\langle C_4 \rangle$ (average obtained over 100 network realizations) on the network degree d is shown in Figure 7.8. Indeed, the density $\langle C_4 \rangle$ becomes nonzero already below the theoretical threshold d_t, supporting the early appearing changes in the

trends shown in Figure 7.7. As the network degree d increases, the density $\langle C_4 \rangle$ increases exponentially, with the rate of increase becoming slower for larger network size N. For large N, higher network degrees d are needed to obtain the same $\langle C_4 \rangle$.

Since the cycle convergence seems to be associated with the 4-clique density $\langle C_4 \rangle$, instead of comparing networks with different size N for the same degree d (which also depends on N), it seems to be natural to relate networks for the same density $\langle C_4 \rangle$. In the following, therefore, cyclic behaviors for different N will be compared by investigating dependences of the transient and subharmonic lengths on the 4-clique density $\langle C_4 \rangle$.

7.4.2 Divergent transient length

Figure 7.9(a) shows a log-log plot of the t_T vs. $\langle C_4 \rangle$ dependence. The transient length increases with the number of cliques following a power law behavior, with slope increasing with the size N. As seen from the figure, a twofold increase of N results in roughly 10-fold increase t_T. On the other hand, Figure 7.9(b) shows only less than a twofold increase of the subharmonic period t_S. Therefore, due to the slow growth of t_S, no conclusions can be made regarding the behavior of the subharmonic cycle length in the thermodynamic limit ($N \to \infty$). On the other hand, the transient length t_T shows more rapid growth. Dependence of t_T on the network size N is plotted in Figure 7.10 for different 4-clique densities $\langle C_4 \rangle$. Data have been fitted very well by exponential law $\langle t_T \rangle \approx \exp(N/\tau)$ with τ being the fitting parameter. As $\langle C_4 \rangle$ decreases the slope and the curvature of the exponential function decreases. This is confirmed in the inset in Figure 7.10 showing dependence of the fitting parameter τ on $\langle C_4 \rangle$, where $\tau \to \infty$ in the limit $\langle C_4 \rangle \to 0$. This means that for $d > d_t$, when 4-cliques emerge and C_4 becomes nonzero, the $\langle t_T \rangle$ grows faster than N, implying that hysteretic trajectories will not converge in the limit ($N \to \infty$).

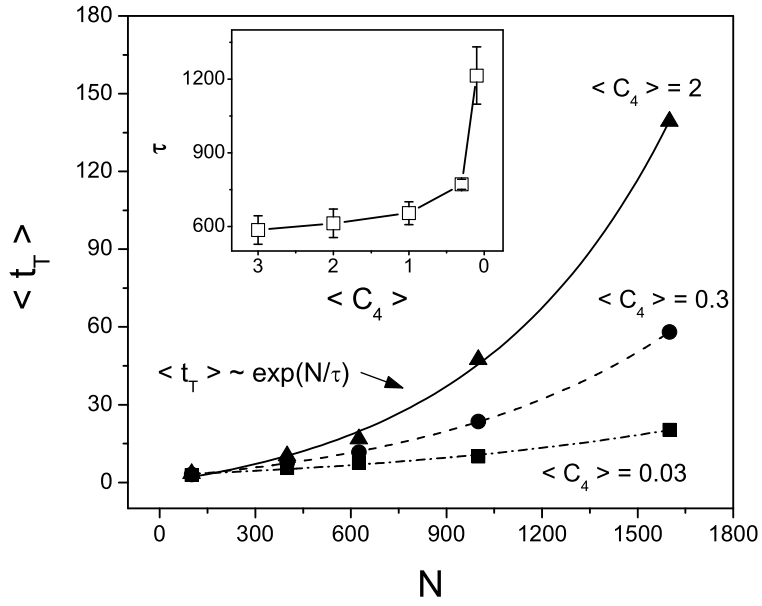

Figure 7.10: Transient length $\langle t_T \rangle$ as a function of a network size N obtained for $\langle C_4 \rangle = 0.03$, 0.3 and 2. Lines for different $\langle C_4 \rangle$ are exponential fits. Inset: dependence of the exponential fit parameter τ on $\langle C_4 \rangle$. τ grows without bound as the density of 4-cliques C_4 decreases. Data corresponds to reversal magnetization $M_r = 0.2$, $\Delta/\sigma = 10$, and $\sigma = 0.1$. Averages are obtained over 100 realizations of randomness.

7.5 Summary

We have demonstrated that the connectivity and the topology of random networks are important factors determining the convergence rate of minor cycles. The main observation is the existence of cycles which do not converge to minor loops after an arbitrarily large number of external field periods. We have shown that such behavior is associated with specific topological elements in the networks structure called cliques of size 4, i.e. the fully interconnected spin groups of size equal or greater than 4. This suggests that behavior of hysteretic cycles could prove to be a useful characterization method for probing topology and connectivity of some systems with complex interactions.

Chapter 8. Hysteretic losses

Hysteresis phenomenon is associated with energy dissipation which is called hysteretic loss [1, 57]. Irreversible thermodynamics of hysteretic systems has been previously developed [94, 95] using an assumption that the difference of losses along upper and lower branches of minor loops is zero. Such an assumption is natural in models ignoring explicit interactions between the components. In this chapter we investigate effects of interactions on the hysteresis loss behavior, using the mean field and the short range interaction RCIS models. Only positive interactions are considered, in order to guarantee the return point memory (RPM) and thus closed minor loops (Figure 8.1). This allows a unique comparison of losses generated for upper and lower minor loop branches.

8.1 Inherent and excess losses: Definition

The expressions for excess losses are derived in a standard way used in thermodynamics [96]. First the inverse Legendre transformation is used to transform the free energy given by Equation 4.3 to $F = G + H \sum s_i$. The change of F due to the flipping of a single switch s_i can the be expressed as

$$dF_i = -ds_i J \sum_j A_{ij} s_j. \tag{8.1}$$

This free energy variation is related to the work performed, Hds_i, and to the internal entropy production δS^P through the well-known thermodynamics relation

$$dF_i = Hds_i - T\delta S_i^P. \tag{8.2}$$

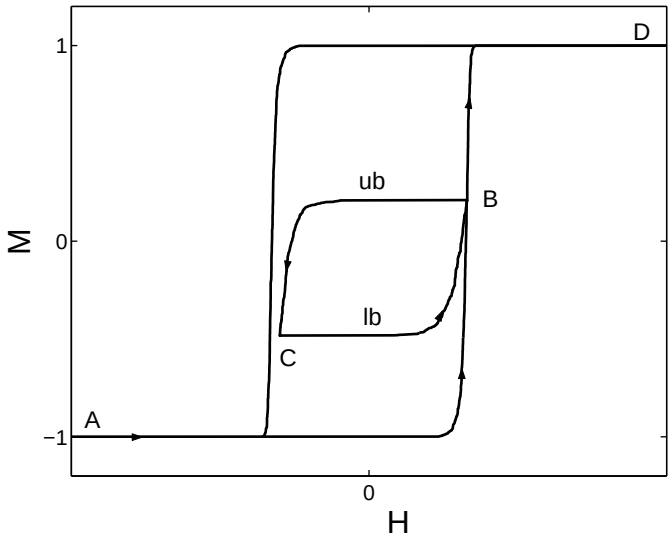

Figure 8.1: Closed loop for a system with return point memory (RPM). The symbols 'ub' and 'lb' denote respectively upper and lower minor loop branches. Are the hysteretic losses corresponding to 'ub' and 'lb' the same?

The energy loss is defined here as $\delta Q_i^T = T\delta S_i^P$. Since each switch can flip only between -1 and $+1$, $ds_i = \pm 2$ in Equations 8.1-8.2 depending on the switching direction. For the very first switch flipping in the avalanche the local field must be equal to its switching threshold. Using this fact together with Equations 4.1-4.2, and 8.2, leads to the following energy loss in flipping the first switch in the avalanche:

$$\delta Q_i^T = H_i^e ds_i = \alpha_i ds_i = 2|\alpha_i| = \delta Q_i^I. \tag{8.3}$$

The amount of this energy loss depends only on the threshold of the first switch. It is completely independent of its interactions with the rest of the system. In fact, this is exactly the loss that would have occurred if the same switch flipped in the absence of any interactions. For this reason this loss is called the inherent loss Q_i^I.

After the first switch flipped in the avalanche, the local field magnitudes at the location of its neighbors increase to match or exceed their thresholds. This difference

between the local field and the thresholds depends on the topology, sign and strength of interactions, and results in the additional contribution to the inherent loss that would have occurred in the absence of any interaction. This loss will be called here the excess loss Q_i^{ES}. Thus, the total loss that occurs in flipping any switch can be split into the inherent and excess loss according to:

$$\delta Q_i^T = H_i^e ds_i = 2|\alpha_i| + \delta Q_i^{ES} = \delta Q_i^I + \delta Q_i^{ES}. \tag{8.4}$$

It is important to stress that interactions can actually affect hysteretic losses in two different ways. On the one hand, interactions play a significant role in determining which switches flip during a given variation of the external field. This is related to the fact that interactions determine the input-output relationship of the system. On the other hand, interactions may affect the amount of loss that occurs when any given switch flips. It is this second more subtle effect that we refer to as the excess loss.

8.2 Hysteretic losses in the mean field RCIS model

The mean field RCIS system, the one where every switch interacts equally with every other switch, has already been discussed in Section 5.2 for negative interactions. Here we calculate hysteretic losses for positive interactions. To keep the free energy finite as the size of the system N increases, the interaction strength has to decrease proportionally as J/N. Using this fact, the free energy change in Equation 8.1 can be written as

$$dF_i = -Jds_i M, \tag{8.5}$$

where $M = N^{-1} \sum s_i$ is the magnetization. Similarly as Equation 5.3, the magnetization can be written self-consistently as

$$M = \hat{P}[H + JM], \tag{8.6}$$

where $\hat{P}$ is the Preisach operator. For finite N, switching events appear as magnetization discontinuities in the input-output relation for this system. However, as N increases to infinity, the relationship between M and H becomes smooth (until certain critical interaction strength is reached [70]). Assuming the existence of inverse operator $\hat{P}^{-1}$ in this case, the equation above can be inverted to give $H = \hat{P}^{-1}[M]$. Substituting this inverse and Equation 8.5 into Equation 8.6, and integrating over the magnetization change from M_1 to M_2 leads to energy loss

$$\Delta Q_{12}^{T} = \int_{M_1}^{M_2} \hat{P}^{-1}[M]\, dM. \tag{8.7}$$

This result depends only on switches flipped from state M_1 to state M_2. The only effect of interactions is to determine what field variation actually leads to the given magnetization change. Losses that occur for any given change of magnetization are exactly the same that would have occurred in the absence of any interactions. For this reason, it can be concluded that only inherent losses exist.

We have also performed numerical simulations on this system, details of which are not presented here. The simulations show that excess losses are present for relatively small system size, but approach zero rapidly as the system size increases. This can be understood in the context of the discussion preceding Equation 8.5. When the size of the system is finite, each switch contributes a finite amount to the local field of other switches. Due to the discrete nature of the system, the probability that the local field exceeds the threshold of a given switch by a finite amount at the time of flipping is non-zero. However, as the size of the system N increases, the contribution of each switch to this excess local field diminishes as $J/N \to 0$. In the limit of an infinitely large system, the analytical result in Equation 8.7 becomes valid and the only possible losses are the inherent ones.

8.3 Hysteretic losses in the RCIS model with short range interactions

Free energy change for RCIS with the nearest neighbor interactions is obtained from Equation 8.1 and can be written as

$$dF_i = -Jds_i \sum_{\langle ij \rangle} s_j, \tag{8.8}$$

where the sum is over the nearest neighbors. Inserting Equation 8.8 and Equations 4.1-4.2 into Equation 8.4 and summing up through all switches in an avalanche (state change from M_1 to M_2), the expression for the total loss can be written as follows:

$$\Delta Q_{12}^T = 2\sum_{k=1}^{K_a} \left|\alpha_k\right| + 2\sum_{k=1}^{K_a} \left(\left| J \sum_{\langle kj \rangle} s_j^k + H \right| - \left|\alpha_k\right| \right), \tag{8.9}$$

where index k denotes the state prior to the k-th switch flipping. The first sum is the inherent loss corresponding to the K_a switches flipping in avalanche, whereas the second sum is the excess loss (obtained by subtracting the inherent loss from the total loss defined by Equations 8.3-8.4).

Both inherent and excess energy losses have been calculated numerically using Equation 8.9. Two dimensional rectangular lattice RCIS model where each switch interacts with its 4 nearest neighbors, was simulated for system sizes varying from $N = 10^3$ to $N = 10^4$, threshold variance $\sigma = 1$ and mean $\mu = 4$ and 6 (we assume $\mu > 3\sigma$ in order to preserve Gaussian profile of a threshold distribution). Distribution functions for avalanche sizes $D(\Delta M)$, inherent $D(\Delta Q^I)$ and excess $D(\Delta Q^{ES})$ losses occurring during the avalanches have been obtained along the increasing branch of the major hysteresis loop for different interaction strengths (Figure 8.2. shows two examples). Avalanche sizes ΔM span several decades and increase with ratio J/σ yielding increase of the amount of both inherent and excess loss. Moreover, inherent losses increase with μ, whereas excess losses are not dependent on the average thresh-

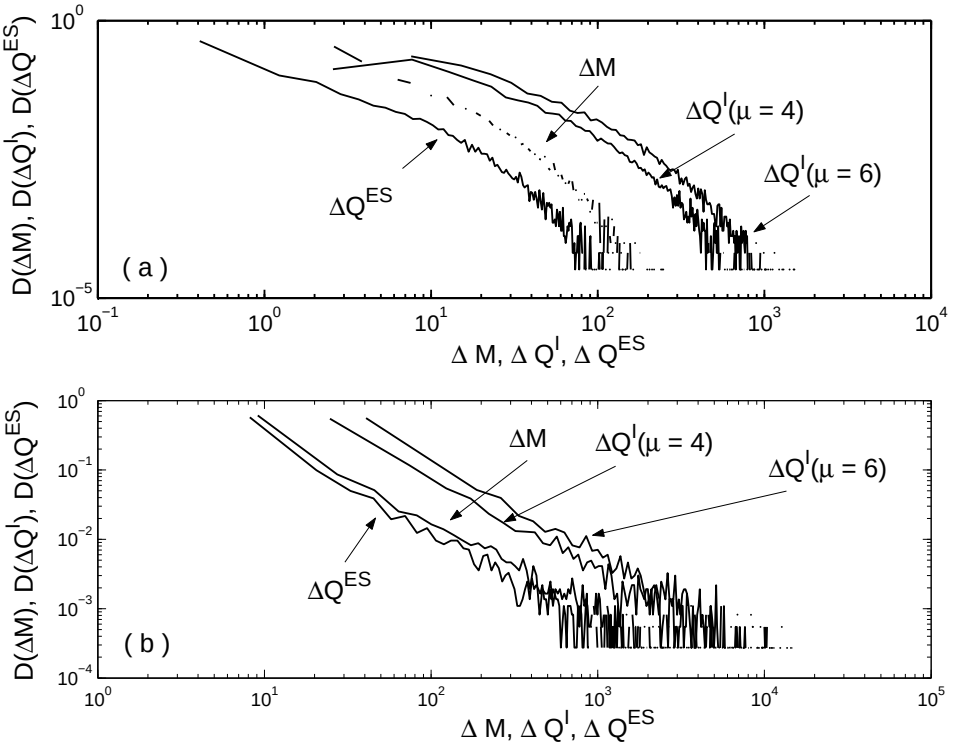

Figure 8.2: Distribution functions D for avalanches ΔM, inherent losses ΔQ^I, and excess losses Q^{ES} generated for 2 dimensional 40×40 spin RCIS with $\sigma = 1$ and $\sigma = 4$ and 6 (Gaussian distribution of thresholds) and 100 realizations of disorder. (a) $J = 0.5$, (b) $J = 1.0$.

old μ. Numerical simulations confirm that energy losses depend on the ratio J/σ. Thus, increasing the interaction strength is equivalent to decreasing the disorder and vice versa. All distribution functions begin to follow the same power law behavior at an interaction exceeding about $J/\sigma = 1$. Previously, using RFIM, power law scaling of avalanche sizes has been shown to be a manifestation of a nearby critical point with disorder and external field as tuning parameters [69]. In this respect, RCIS system probably belongs to the same universality class as the RFIM. Although we did not attempt to carry out precise observations, the critical interaction strength seems to occur around $(J/\sigma)_{\rm crit}$.

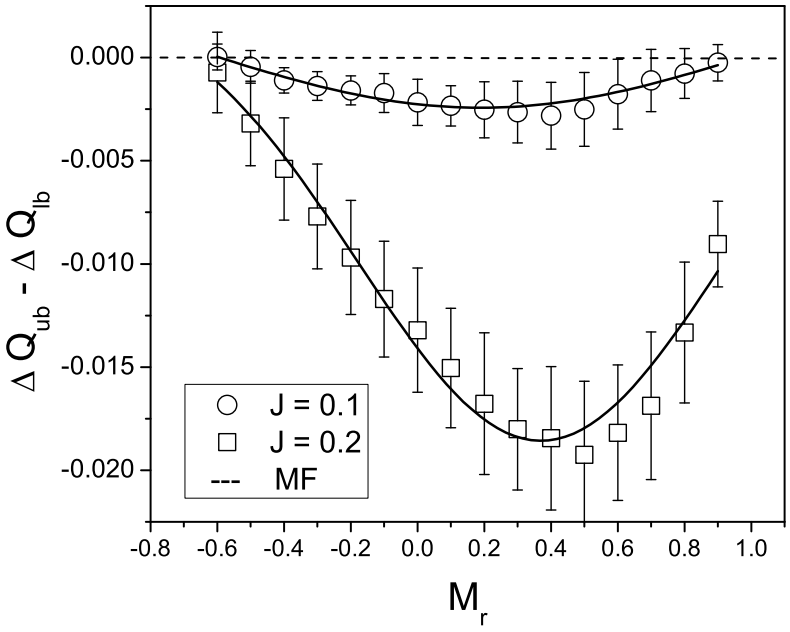

Figure 8.3: Difference between hysteretic losses generated during the upper and lower minor loop branches for different reversal points $M_r(H_r)$ on the major hysteresis loop. Only minor loops with symmetric reversal points $H_d = -H_r$ are assumed. The data was averaged over 20 realizations of randomness. The dashed line denotes a zero loss difference obtained for the mean field RCIS model.

8.4 Hysteretic losses produced during minor cycles

Due to RPM property, the same spins flipping down during the decreasing minor loop branch must flip up during the lower minor loop branch. As a result, the inherent losses for the upper and lower branches are the same, and any existing differences between the hysteretic losses generated for upper and lower minor loop branches must be attributed to the presence of excess losses. Note, that since excess losses do not exist in the case of the mean field RCIS model, the loss differences are zero (dashed line in Figure 8.3). For a RCIS model with the nearest neighbor interactions, we studied the loss differences for a set of minor loops with symmetric reversal points

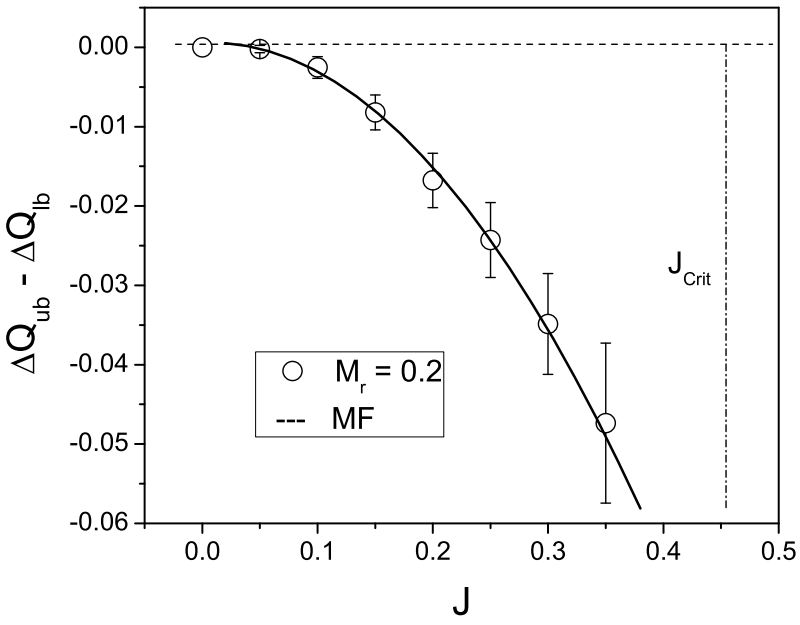

Figure 8.4: Difference between hysteretic losses for upper and lower minor loop branches vs. the interaction strength. Data was averaged over 20 realizations of randomness. Dashed line denotes a zero loss difference obtained for the mean field RCIS model.

$H_d = -H_r$ attached to major hysteresis. As shown in Figure 8.3 for two different interaction magnitudes, the loss difference increases with the reversal magnetization $M_r(H_r)$, reaching the peak after the major loop coercive point and starts to decrease to zero. Note, that doubling the interaction magnitude increases the loss difference by a factor of about 7.

The dependence on the interaction strength for a fixed disorder is shown in Figure 8.4 for a minor loop with reversal magnetization $M_r = 0.2$. The difference between the excess losses for 'ub' and 'lb' increases rapidly with the interaction strength, until the critical point is reached. After the critical interaction, the entire system switches in one large avalanche that occurs along the major loop. Minor loops inside the major loop either do not exist or are hard to reach [97]. Consequently, the losses obtained

for interaction strengths above the critical point J_{crit} are equal along the lower and upper branches of the major loop.

8.5 Summary

Switching events in many systems are normally associated with hysteretic losses even when no interactions within the system exist. In this chapter, we demonstrated that interactions can contribute additional losses during the switching events. Such excess losses can play important role in systems with local interactions, and as shown here behave asymmetrically for upper and lower minor loop branches, which contradicts traditional thermodynamic models of hysteresis. In case of the mean field interactions, excess losses do not exist and losses generated during the minor loop branches are equal. Understanding the origins of the loss asymmetry in short interaction range models will be a subject of future research.

Chapter 9. Concluding remarks

9.1 Summary and conclusions

In this thesis we investigated the hysteretic processes (rate independent irreversible processes) generated by a cyclically varying scalar parameter. The main goal was to understand how the qualitative behavior of hysteresis cycles depends on the structure of interactions between the basic elements of the system.

Motivated by available experimental results and by standard models, we developed the Random Coercivity Interacting Switch model (RCIS) which we then used as a paradigm for complex systems with scalar hysteresis. The basic building blocks of the model are the bistable spins with elementary rectangular hysteresis loops. Disorder in the system is modeled by assuming random widths of the hysteresis loops of individual spins. In addition, we assumed that the spins interact via a network of pair-wise interactions. When compared to traditional models of hysteresis, such as RFIM for example, the main new property of the RCIS model is the existence of a simple dynamical regime for weak negative interactions. The main characteristic of this regime is trivial avalanches generated by spins flipping one by one along the field direction, similarly to magnetic domains in media with very strong anisotropies. In this 'single spin flip' dynamical limit, convergence to a unique state is guaranteed for any interaction range and topology. This permits to overcome problems with mathematical consistency often appearing in models of hysteresis with negative interactions. As shown in this thesis, even this simple single spin flip dynamics produces nontrivial behavior of minor cycles, ranging from closed minor loops to never stabilizing cycles.

The starting point was the investigation of origins of the cycle opening in the RCIS model. It was shown in Chapter 5 that as long as the interactions are positive

(i.e. favoring parallel alignment of neighboring spins), minor cycles produce closed hysteresis loops at the end of the very first cycle independently of the structure of interaction network. Although this is generally not the case if interactions are negative (favoring anti-parallel alignment of neighboring spins), still there exist some negative interaction networks where closure of the minor cycles occurs at the end of the first cycle. We gave two examples: 1) the mean field RCIS model, where every spin interacts equally with every other spin, and 2) the Néel's type mean field RCIS model, where spins were divided into two groups with interactions between these two groups only. While in the first case the minor cycles remain closed independently of the interaction strength, in the second case there exists a certain interaction strength at which open cycles suddenly emerge. Then, as the interaction strength increases, minor cycles remain open and several external field cycles are required for the minor loop formation. We found that the value of the critical interaction depends on the variance of the spin-threshold distribution and therefore is fundamentally associated with the presence of the disorder. The main difference between the fully connected and the Néel's type mean field models is in the number of variables required for full characterization of the state. In the first case, it is sufficient to specify a single variable corresponding to the average spin state (magnetization). In the second case two state variables are necessary, each corresponding to the average spin state of the particular spin group. Cycle opening appears at a critical interaction as soon as one state variable begins to lag after the other. Based on this analysis we conclude that there are two necessary conditions for existence of open cycles: 1) negative interactions between the spins, and 2) the state of the system is described by at least two independent variables (although some very simple two-state-variable systems, such as a spin couple, still display only closed cycles).

As an opposite limit of the mean field (fully connected network) models, we considered a class of models with short range interactions, where each spin interacts with

only a few neighbors (Chapter 6). One example is the RCIS model with spins distributed on a two-dimensional lattice and negative interactions extending only between the nearest neighbors. Note that in this case, the state is completely characterized only after specifying the state of each individual spin. The main difference here seems to be the absence of sharp appearance of the cycle opening at any interactions strength. Instead, we observed that for a given interaction strength and disorder level, there always exists a particular realization of the randomness for which an open cycle can be found. The number of open cycles for a given number of realizations of randomness depends on the interaction strength relative to variance of the disorder. Openings are rarely observed if interactions are weak.

Analysis of the origins of cycle opening in the short range lattice models can be simplified by considering an approximation that divides the lattice into independent spin-triplets. Such an ensemble of independent triplets is the simplest system producing open cycles (independent spin-couples produce closed minor loops). Additionally, since any long range correlations are impossible, the opening must be due to the inherent properties of individual triplets. Indeed, as it turns out, only triples with specific arrangement of thresholds contribute to cycle opening of the entire ensemble. Detailed analysis revealed that there are two mechanisms yielding the cycle opening. The first mechanism produces open cycles where the magnetization difference after the cycle equals to the spin state difference. The second mechanism produces open cycles, where the magnetization difference after the cycle equals zero, but the spin state difference is nonzero. We find that, while both mechanisms are coupled if external field cycles between symmetric reversal points, only the first mechanism exists for cycles with the lower reversal magnitude sufficiently smaller than the magnitude of the upper reversal. This shows the fundamental difference between the symmetric and non-symmetric minor cycles. We then derived the dependence of the cycle opening on the interaction and variance, which proves that the loop opening decreases

continuously to zero as the interaction strength reduces to zero at a given variance of the disorder. This conclusion is consistent with the short interaction range lattice model. The possibility of the correlation effects in the lattice models, if any, will be a subject of future investigations.

Based on the analysis of the mean field and short interaction range RCIS models, as two opposite limits of the network connectivity, it became clear that the network connectivity plays a crucial role in determining the behavior of cycles. In Chapter 7 we investigated the effects of interaction structure on the cycle opening assuming RCIS model on a random network. Random networks are convenient since their connectivity and topology can be tuned between the sparse and fully connected limits via a single parameter; hence they are often employed as a paradigm for studying complex systems. We considered cycles with symmetric reversal points and given the conclusions from the analysis of the ensemble of triplet model, measured the cycle opening by comparing the microstates before and after the cycle. As demonstrated, when the network connectivity is sparse, minor cycles converge quickly to stable minor loops. As the network connectivity increases, the convergence rate decreases. At a certain connectivity degree, non-convergent minor cycles appear which do not form closed minor loops after an arbitrarily large number of external field periods. As we find, the emergence of the non-convergent loops is associated with the presence of specific topological elements in the network structure, particularly the cliques (complete subgraphs) of size 4. This conclusion suggests that behavior of hysteretic cycles could prove to be a useful characterization method for probing topology and connectivity of some systems with complex interactions. We note that the average state (magnetization) in our simulations did not show the same behavior as the microscopic state.

Finally, we examined effects of the interaction structure on certain thermodynamic aspects of hysteresis, particularly behavior of hysteretic losses. First we showed that for any interaction network it is convenient to separate total loss into two parts:

1) the inherent loss, associated only with the elements composing the system and present even in the absence of interactions and 2) excess losses being solely due to the interactions. Excess losses are absent for negative interactions in the single spin flip dynamics limit. For this reason, we analyzed only the RCIS model with positive interactions. We then considered mean field and the nearest neighbor RCIS models with positive interactions, as two opposite limits of the network connectivity. It was shown that while the inherent losses are present in both models, the excess losses exist only for the RCIS model with the nearest neighbor interactions. In addition, excess hysteresis losses due to the interactions introduce additional effects which have been ignored in traditional models describing thermodynamics of hysteretic processes. Example of such an effect is the different amount of losses generated during increasing and decreasing branches of non-symmetric minor loops. These results support the fact, that a proper thermodynamic description of hysteresis phenomena is still an open problem.

9.2 Future outlook

In the future, this work will be extended into several different directions in both basic and applied science. Several works already in progress are listed below.

1. Why we do not observe drifting R-type cycles? The models studied in this thesis consisting of bistable spins with either positive or negative interactions did not reproduce the creeping R-type cycles (Figure 9.1), which are frequently observed for example in magnetism and referred to as reptation effects. This suggests that in order to observe the R-type cycles, the present models have to be generalized either to 1) spin networks with both positive and negative interactions, or 2) spin networks with multi-stable components and components of a vector nature. Such models are also more realistic descriptions of many material systems. Another interesting question

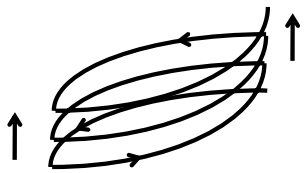

Figure 9.1: R-type cycle. Reversal points move in the same direction after every external field period (see also Figure 2.3).

is how to properly quantify cyclic behaviors using macroscopic measurements. In Section 7.3.2, we saw that cycle opening measured as a difference between magnetizations before and after the cycle often yields noisy results. Our future goal is to analyze the statistical properties of fluctuations of the various macroscopic measures, and identify their relations with the structure of the system.

2. Identification of structures of realistic complex networks. The observation that hysteretic trajectories depend on the topological elements present in the network structure stimulates search for universal relationships between the rich variety of qualitative hysteretic behaviors, and properties of underlying interaction networks [98]. In this thesis we focused on systems where spins are distributed on regular networks (lattices) and then on networks modeled by classical random graphs, which are the simplest and most straightforward realizations of complex networks. Future research will concentrate on realistic networks with less trivial organizing principles, such as the scale free and small world networks [87]. Scale free networks are characterized by degree distributions with power law tails and we expect dependence of hysteretic behavior, such as e.g. the rate of the minor loop formation, on the associated power law exponent. Another class of systems of interest is the small world network which allows interpolating between the lattices and classical random networks and thus tuning the average path length and the clustering coefficient. These properties are also expected to influence hysteresis. We also want to investigate effects of the presence of various

topological elements in the network such as trees, cycles, or complete sub-graphs. The main motivation behind these studies is to develop a universal framework for relating qualitative features of processes and the structure of networks for a broad class of complex systems.

3. Patterned magnetic nanostructures. The modeling approach used in this thesis is very convenient for modeling hysteresis behaviors of various types of magnetic nanostructures. Patterned magnetic nanostructures are important for technological applications such as magnetic recording technology, sensors, MRAM, and magneto-electronics. Developing these applications, however, relies on understanding and control of interactions in these structures, such as the local exchange interactions, for instance. Interaction effects become particularly pronounced as the distance between different features of the nanostructures decreases. These effects are typically manifested by changes of macroscopic magnetic characteristics such as coercivity, switching field dispersion, presence of induced anisotropies, etc. Our future goal is to analyze links between the magnetic properties and the structure of patterned media including the topological distribution and properties of individual elements, disorder and size effects.

It is also of practical interest to understand the various dynamical and memory aspects of hysteresis in patterned nanostructures, particularly the ability or inability to recover their state for cyclically varying external fields. It becomes clear, based on the results presented in this thesis that depending on the 'design' of the structure, it is possible to observe either exact state recovery after every field period or a gradual cycle closure extending over several periods. Since the state-pattern changes during each cycle, the state of the patterned media could in principle be programmed by only very simple external field histories such as a periodically varying external field. After understanding the fundamental principles, e.g. the state vs. cycle number dependence on interactions and disorder, it would be possible to fabricate programmable

sensors suitable for biological and medical applications and to develop assembly techniques directed by only uniform external fields. Ability to control information stored using relatively uniform fields may have profound consequences for information storage industry.

4. Applications to Spintronics. We also started to apply the computational modeling approach developed in this thesis to understanding the physics of coupled ferromagnetic bilayers [34, 99–101]. Such structures can be viewed as a model system for wider class of materials with exchange bias (Section 2.3). The goal is to understand 1) the origin of exchange bias, which is typically manifested by shifted and deformed hysteresis loops, and 2) the origin of training effects where the loop shift changes with external field periods. The training effects are analogous to R-type cyclic behavior shown in Figure 9.1. Our modeling efforts will permit design of novel exchange bias characterization techniques. Magnetic multilayers are interesting from a fundamental as well as technological viewpoint. Ferromagnetic multilayers have been utilized as disk recording media for the past five years due their superior stability and performance characteristics. They are also used in Spintronic applications such as spin valves, for example, and considered as candidates for developing MRAM technology.

Bibliography

[1] G. Bertotti, *Hysteresis in Magnetism: For Physicists, Material Scientists, and Engineers*. Academic Press, San Diego, 1998.

[2] D. Spasojević, S. Bukvić, S. Milošević, and H. E. Stanley, "Barkhausen noise: Elementary signals, power laws, and scaling relations," *Physical Review E*, vol. 54, pp. 2531–2546, 1996.

[3] J. R. Petta, M. B. Weissman, and G. Durin, "Dependence of Barkhausen pattern reproducibility on hysteresis loop size," *Physical Review E*, vol. 56, pp. 2776–2780, 1997.

[4] P. Fischer, T. Eimüller, G. Schütz, P. Guttmann, G. Schmahl, K. Pruegl, and G. Bayreuther, "Imaging of magnetic domains by transimission x-ray microscopy," *Journal of Physics D: Applied Physics*, vol. 31, pp. 649–655, 1998.

[5] M. S. Pierce, R. G. Moore, L. B. Sorensen, S. D. Kevan, O. Hellwig, E. E. Fullerton, and J. B. Kortright, "Quasistatic x-ray speckle metrology of microscopic magnetic return-point memory," *Physical Review Letters*, vol. 90, pp. 175502(1–4), 2003.

[6] M. S. Pierce, C. R. Buechler, L. B. Sorensen, J. J. Turner, S. D. Kevan, E. A. Jagla, J. M. Deutsch, T. Mai, O. Narayan, J. E. Davies, K. Liu, J. H. Dunn, K. M. Chesnel, J. B. Kortright, O. Hellwig, and E. E. Fullerton, "Disorder-induced microscopic magnetic memory," *Physical Review Letters*, vol. 94, pp. 017202(1–4), 2005.

[7] L. P. Lévy, "Reptation and hysteresis in disordered magnets," *J. Phys. I France*, vol. 3, pp. 533–557, 1993.

[8] P. J. Thompson and R. Street, "Reptation and magnetic viscosity effects in a permanent magnet," *Journal of Physics D*, vol. 29, pp. 2789–2795, 1996.

[9] V. Hajko, J. Daniel-Szabó, L. Potocký, and A. Zentko, "Some special cases of the magnetization processes of ferromagnets," *IEEE Transactions on Magnetics*, vol. MAG-10, pp. 128–132, 1974.

[10] E. D. Torre, *Magnetic Hysteresis*. Piscataway, NJ: IEEE Press, 2000.

[11] E. D. Torre, L. Yanik, A. E. Yarimbiyik, and M. J. Donahue, "Differential equation model for accommodation magnetization," *IEEE Transactions on Magnetics*, vol. 40, pp. 1499–1505, 2004.

[12] L. Néel, "On the effects of a coupling between ferromagnetic grains exhibiting hysteresis," *Comptes Rendus*, vol. 246, pp. 2313–2316, 1958.

[13] L. Néel, "Coupling between elementary ferromagnetic domains: Tilting effect," *Comptes Rendus*, vol. 246, pp. 2963–2965, 1958.

[14] L. Néel, "The effects of interactions between elementary ferromagnetic domains: Tilting and creep," *Journal de Physique et le Radium*, vol. 20, pp. 215–221, 1959.

[15] L. Néel, "An attempt to interpret the creep in hysteresis loops," *Comptes Rendus*, vol. 244, pp. 2668–2671, 1957.

[16] P. I. M. V. G. Lewis and K. OGrady, "Reptation effects in particulate systems. II. Experimental studies," *Journal of Applied Physics*, vol. 73, pp. 6656–6658, 1993.

[17] L. H. Bennett, L. J. Swartzendruber, F. Vajda, E. D. Torre, and J. H. Judy, "Aftereffect and accommodation anisotropy in metal-particle and metal-evaporated recording media," *IEEE Transactions on Magnetics*, vol. 33, pp. 4173–4175, 1997.

[18] J. Martín, J. Nogués, K. Liu, J. Vicent, and I. K. Schuller, "Ordered magnetic nanostructures: fabrication and properties," *Journal of Magnetism and Magnetic Materials*, vol. 256, pp. 449–501, 2003.

[19] T. G. Sorop, C. Untiedt, F. Luis, M. Kröll, M. Rasa, and L. J. de Jongh, "Magnetization reversal of ferromagnetic nanowires studied by magnetic force microscopy," *Physical Review B*, vol. 67, pp. 014402(1–8), 2003.

[20] M. P. Horvath, G. Zheng, and G. Vertesy, "Magnetization process in a classical system of Preisach type particles," *Physica B*, vol. 233, pp. 287–293, 1997.

[21] R. F. Wang, C. Nisoli, R. S. Freitas, J. Li, W. McConville, B. J. Cooley, M. S. Lund, N. Samarth, C. Leighton, V. H. Crespi, and P. Schiffer, "Artificial 'spin ice' in a geometrically frustrated lattice of nanoscale ferromagnetic islands," *Nature*, vol. 439, pp. 303–306, 2006.

[22] J. M. Deutsch, T. Mai, and O. Narayan, "Hysteresis multicycles in nanomagnet arrays," *Physical Review E*, vol. 71, pp. 026120(1–7), 2005.

[23] W. H. Meiklejohn and C. P. Bean, "New magnetic anisotropy," *Physical Review*, vol. 102, pp. 1413–1414, 1956.

[24] J. Nogués and I. K. Schuller, "Exchange bias," *Journal of Magnetism and Magnetic Materials*, vol. 192, pp. 203–232, 1999.

[25] A. E. Berkowitz and K. Takano, "Exchange anisotropy - a review," *Journal of Magnetism and Magnetic Materials*, vol. 200, pp. 552–570, 1999.

[26] M. R. Fitzsimmons, P. Yashar, C. Leighton, I. K. Schuller, J. Nogués, C. F. Majkrzak, and J. A. Dura, "Asymmetric magnetization reversal in exchange-biased hysteresis loops," *Physical Review Letters*, vol. 84, pp. 3986–3989, 2000.

[27] C. Leighton, M. R. Fitzsimmons, P. Yashar, A. Hoffmann, J. Nogués, J. Dura, C. F. Majkrzak, and I. K. Schuller, "Two-stage magnetization reversal in exchange biased bilayers," *Physical Review Letters*, vol. 86, pp. 4394–4397, 2001.

[28] C. Binek, *Ising Type Antiferromagnets*. Springer, Berlin, 2003.

[29] A. Hoffmann, "Symmetry driven irreversibilities at ferromagnetic-antiferromagnetic interfaces," *Physical Review Letters*, vol. 93, pp. 097203(1–4), 2004.

[30] E. E. Fullerton, D. T. Margulies, M. E. Schabes, M. Carey, B. Gurney, A. Moser, M. Best, G. Zeltzer, K. Rubin, H. Rosen, and M. Doerner, "Antiferromagnetically coupled recording media layers for thermally stable high-density recording," *Applied Physics Letters*, vol. 77, pp. 3806–3808, 2000.

[31] A. Berger, D. T. Margulies, and H. Do, "Magnetic hysteresis loop tuning in antiferromagnetically coupled bilayer structures," *Applied Physics Letters*, vol. 85, pp. 1571–1573, 2004.

[32] C. Binek, S. Polisetty, X. He, and A. Berger, "Exchange bias training effect in coupled all ferromagnetic bilayer structures," *Physical Review Letters*, vol. 96, pp. 067201(1–4), 2006.

[33] A. Berger, C. Binek, D. T. Margulies, A. Moser, and E. E. Fullerton, "Reversible hysteresis loop tuning," *Physica B*, vol. 372, pp. 168–172, 2006.

[34] O. Hovorka, A. Berger, and G. Friedman, "Preisach model of exchange bias in antiferromagnetically coupled bilayers," *IEEE Transactions on Magnetics*, vol. 42, pp. 3129–3131, 2006.

[35] K. H. Fischer and J. A. Hertz, *Spin Glasses*. Cambridge University Press, 1993.

[36] F. Pázmándi, G. Zaránd, and G. T. Zimányi, "Self-organized criticality in the hysteresis of the Sherrington-Kirkpatrick model," *Physical Review Letters*, vol. 83, pp. 1034–1037, 1999.

[37] J. M. Deutsch and O. Narayan, "Subharmonics and aperiodicity in hysteresis loops," *Physical Review Letters*, vol. 91, pp. 200601(1–4), 2003.

[38] C. P. Bean, "Magnetization of hard superconductors," *Physical Review Letters*, vol. 8, pp. 250–253, 1962.

[39] C. P. Poole, *Handbook of Superconductivity*. Academic Press, 2000.

[40] I. D. Mayergoyz and T. A. Keim, "Superconducting hysteresis and the Preisach model," *Journal of Applied Physics*, vol. 67, pp. 5466–5468, 1990.

[41] G. Friedman, L. Liu, and J. S. Kouvel, "Experimental testing of applicability of the Preisach hysteresis model to superconductors," *Journal of Applied Physics*, vol. 75, pp. 5683–5685, 1994.

[42] R. A. Guyer and P. A. Johnson, "Nonlinear mesoscopic elasticity: Evidence for a new class of materials," *Physics Today*, vol. April, pp. 30–36, 1999.

[43] K. McCall and R. A. Guyer, "Equation of state and wave propagation in hysteretic nonlinear elastic materials," *Journal of Geophysical Research*, vol. 99, pp. 23887–23897, 1994.

[44] R. A. Guyer, K. R. McCall, and G. N. Boitnott, "Hysteresis, discrete memory, and nonlinear wave propagation in rock: A new paradigm," *Physical Review Letters*, vol. 74, pp. 3491–3494, 1995.

[45] R. A. Guyer and P. A. Johnson, "Hysteresis, energy landscapes and slow dynamics: A survey of elastic properties of rocks," *Materials Processing and Manufacturing Science*, vol. 9, pp. 14–26, 2000.

[46] D. H. Everett, *The Solid Gas Interface*, vol. 2. Marcel Dekker, New York, 1967.

[47] M. P. Lilly, P. T. Finley, and R. B. Hallock, "Memory, congruence, and avalanche events in hysteretic capillary condensation," *Physical Review Letters*, vol. 71, pp. 4186–4189, 1993.

[48] D. J. Tulimieri, J. Yoon, and M. H. W. Chan, "Ordering of helium mixtures in porous gold," *Physical Review Letters*, vol. 82, pp. 121–124, 1999.

[49] E. Kierlik, P. A. Monson, M. L. Rosinberg, L. Sarkisov, and G. Tarjus, "Capillary condensation in disordered porous materials: Hysteresis versus equilibrium behavior," *Physical Review Letters*, vol. 87, pp. 055701(1–4), 2001.

[50] E. Kierlik, P. Monson, M. Rosinberg, and G. Tarjus, "Adsorption hysteresis and capillary condensation in disordered porous solids: a density functional study," *Journal of Physics: Condensed Matter*, vol. 14, pp. 9295–9315, 2002.

[51] F. Detcheverry, E. Kierlik, M. L. Rosinberg, and G. Tarjus, "Hysteresis in capillary condensation of gases in disordered porous solids," *Physica B*, vol. 343, pp. 303–307, 2004.

[52] L. Piscitelli, M. Grinfeld, H. Lamba, and R. Cross, "On entry and exit in response to aggregate shocks," *Applied Economics Letters*, vol. 6, pp. 569–572, 1999.

[53] M. Göcke, "Various concepts of hysteresis in economics," *Journal of Economics Surveys*, vol. 16, pp. 1–21, 2002.

[54] L. Piscitelli, R. Cross, M. Grinfeld, and H. Lamba, "A test for strong hysteresis," *Computational Economics*, vol. 15, pp. 59–78, 2000.

[55] M. Grinfeld, L. Piscitelli, and R. Cross, "A probabilistic framework for hysteresis," *Physica A*, vol. 287, pp. 577–586, 2000.

[56] M. Brokate and J. Sprekels, *Hysteresis and Phase Transitions*. Springer, New York, 1996.

[57] G. Bertotti and I. D. Mayergoyz, *Science of Hysteresis*. Academic Press, 2006.

[58] F. Liorzou, B. Phelps, and D. L. Atherton, "Macroscopic models of magnetization," *IEEE Transactions on Magnetics*, vol. 36, pp. 418–428, 2000.

[59] D. C. Jiles, "Theory of ferromagnetic hysteresis," *Journal of Applied Physics*, vol. 55, pp. 2115–2120, 1984.

[60] F. Preisach, "Über die magnetische nachwirkung," *Zeitschrift für Physik*, vol. 94, pp. 277–302, 1935.

[61] J. P. Sethna, K. A. Dahmen, and O. Perković, "Random-field Ising models of hysteresis," *Cond-Mat*, vol. 0406320, pp. 1–33, 2004.

[62] M. Brokate and E. D. Torre, "The wiping-out property of the moving model," *IEEE Transactions on Mangnetics*, vol. 27, pp. 3811–3814, 1991.

[63] I. D. Mayergoyz, "Mathematical models of hysteresis," *Physical Review Letters*, vol. 56, pp. 1518–1521, 1986.

[64] G. Bertotti, V. Basso, C. Beatrice, M. LoBue, A. Magni, and P. Tiberto, "Hysteresis in magnetic materials: the role of structural disorder, thermal relaxation, and dynamic effects," *Journal of Magnetism and Magnetic Materials*, vol. 226, pp. 1206–1212, 2001.

[65] I. D. Mayergoyz, *Mathematical Models of Hysteresis*. Academic Press, 2003.

[66] G. Friedman, "Method for characterization of hysteresis in two dimensions," *IEEE Transactions on Magnetics*, vol. 36, pp. 216–222, 2000.

[67] G. Friedman, K. Cha, Y. Huang, and J. Kouvel, "Vector form of wipe-out memory and its experimental testing," *IEEE Transactions on Magnetics*, vol. 36, pp. 3185–3188, 2000.

[68] Y. Huang, G. Friedman, I. Obeidad, and J. Kouvel, "Experimental identification of the switching field for use in vector hysteresis models," *Journal of Applied Physics*, vol. 87, p. 4777, 2000.

[69] J. P. Sethna, K. A. Dahmen, and C. R. Myers, "Crackling noise," *Nature*, vol. 410, pp. 242–250, 2001.

[70] J. P. Sethna, K. Dahmen, S. Kartha, J. A. Krumhansl, B. W. Roberts, and J. D. Shore, "Hysteresis and hierarchies: Dynamics of disorder-driven first order phase transformations," *Physical Review Letters*, vol. 70, pp. 3347–3350, 1993.

[71] K. Dahmen and J. P. Sethna, "Hysteresis, avalanches, and disorder-induced critical scaling: A renormalization-group approach," *Physical Review B*, vol. 53, pp. 14872–14905, 1996.

[72] P. Shukla, "Exact expressions for minor hysteresis loops in the random field Ising model on a Bethe lattice at zero temperature," *Physical Review E*, vol. 63, pp. 027102(1–4), 2001.

[73] D. Dhar, P. Shukla, and J. P. Sethna, "Zero-temperature hysteresis in the random-field Ising model on a Bethe lattice," *Journal of Physics A*, vol. 30, pp. 5259–5267, 1997.

[74] S. Sabhapandit, P. Shukla, and D. Dhar, "Distribution of avalanche sizes in the hysteretic response of the random-field Ising model on a Bethe lattice at zero temperature," *Journal of Statistical Physics*, vol. 98, pp. 103–129, 2000.

[75] B. Tadić, K. Malarz, and K. Kulakowski, "Magnetization reversal in spin patterns with complex geometry," *Physical Review Letters*, vol. 94, pp. 137204(1–4), 2005.

[76] P. Shukla, "Zero-temperature hysteresis in an anti-ferromagnetic Ising chain with quenched random fields," *Physica A*, vol. 233, pp. 242–252, 1996.

[77] P. Shukla, R. Roy, and E. Ray, "Hysteresis in one-dimensional anti-ferromagnetic random-field Ising model at zero temperature," *Physica A*, vol. 276, pp. 365–375, 2000.

[78] E. Vives and A. Planes, "Hysteresis and avalanches in disordered systems," *Journal of Magnetism and Magnetic Materials*, vol. 221, pp. 164–171, 2000.

[79] J. M. Deutsch, A. Dhar, and O. Narayan, "Return to return point memory," *Physical Review Letters*, vol. 92, pp. 227203(1–4), 2004.

[80] O. Hovorka and G. Friedman, "Onset of reptations and critical hysteretic behavior in disordered systems," *Journal of Magnetism and Magnetic Materials*, vol. 290-291, p. 449, 2005.

[81] H. G. Katzgraber and G. T. Zimanyi, "Hysteretic memory effects in disordered magnets," *Physical Reivew B*, vol. 74, pp. 020405(R)(1–4), 2006.

[82] H. G. Katzgraber, F. Pazmandi, C. R. Pike, K. Liu, R. T. Scalettar, K. L. Verosub, and G. T. Zimanyi, "Reversal-field memory in the hysteresis of spin glasses," *Physical Review Letters*, vol. 89, pp. 257202(1–4), 2002.

[83] E. Vives and A. Planes, "Avalanches in a fluctuationless first-order phase transition in a random-bond Ising model," *Physical Review B*, vol. 50, pp. 3839–3848, 1994.

[84] O. Hovorka and G. Friedman, "Closure of minor hysteresis loops in disordered antiferromagnetic systems," *Journal of Applied Physics*, vol. 97, pp. 10E514–10E516, 2005.

[85] S. N. Dorogovtsev and J. F. F. Mendes, *Evolution of Networks: From Biological Nets to the Internet and WWW*. Oxford University Press, USA, 2003.

[86] B. Bollobás, *Random Graphs*. Cambridge University Press, 2001.

[87] R. Albert and A.-L. Barabási, "Statistical mechanics of complex networks," *Reviews of Modern Physics*, vol. 74, pp. 47–97, 2002.

[88] J. E. Cohen, "Threshold phenomena in random structures," *Discrete Applied Mathematics*, vol. 19, pp. 113–128, 1988.

[89] P. Moriarty, "Nanostructured materials," *Reports on Progress in Physics*, vol. 64, pp. 297–381, 2001.

[90] E. D. Torre, "Effect of interaction on the magnetization of single domain particles," *IEEE Transactions on Audio and Electroacoustics*, vol. 14, pp. 86–92, 1966.

[91] A. H. Morrish, *The Physical Principles of Magnetism*. Wiley-IEEE Press, 2001.

[92] M. A. Krasnoselskii and A. V. Pokrovskii, *Systems with Hysteresis*. Springer, 1989.

[93] N. Goldenfeld, *Lectures on Phase Transitions and the Renormalization Group Theory*. Westview Press, 1992.

[94] I. D. Mayergoyz and G. Friedman, "The Preisach model and hysteretic energy losses," *Journal of Applied Physics*, vol. 61, pp. 3910–3912, 1987.

[95] G. Bertotti, "Energetic and thermodynamic aspects of hysteresis," *Physical Review Letters*, vol. 76, pp. 1739–1742, 1996.

[96] W. Greiner, L. Neise, and H. Stöcker, *Thermodynamics and Statistical Mechanics*. Springer, 2001.

[97] J. H. Carpenter, K. A. Dahmen, J. P. Sethna, G. Friedman, S. Loverde, and A. Vanderveld, "Subloops, Barkhausen noise, and disorder induced critical behavior," *Journal of Applied Physics*, vol. 89, pp. 6799–6801, 2001.

[98] O. Hovorka and G. Friedman, "Non-converging hysteresis cycles in random spin networks," *Cond-mat*, vol. 0703525, pp. 1–4, 2007.

[99] O. Hovorka, A. Berger, and G. Friedman, "Estimation of exchange coupling distribution in all-ferromagnetic bilayers," *IEEE Transactions on Magnetics*, vol. 43, pp. 2953–2955, 2007.

[100] O. Hovorka, A. Berger, and G. Friedman, "Experimental comparison of exchange bias measurement methodologies," *Journal of Applied Physis*, vol. 101, pp. 09E515–09E517, 2007.

[101] O. Hovorka, A. Berger, and G. Friedman, "Center of mass method for exchange bias measurement," *Applied Physics Letters*, vol. 89, pp. 142531(1–3), 2006.

Vita

Ondrej Hovorka

Education

Ph.D. (pending)	Electrical Engineering, Drexel University, Philadelphia, PA, USA, 2003-current
M.S.	Materials Engineering, University of Illinois at Chicago, Chicago, IL, USA, 2002
B.S.	Physics, Comenius University, Bratislava, Slovakia, 2000

Professional Experience

- Drexel University, Department of Electrical and Computer Engineering
  - 9/2002-present: Graduate Research Assistant to Dr. G. Friedman
  - 1/2004-9/2004: Teaching Assistant to Dr. E. Gerber
- University of Illinois at Chicago, Department of Civil and Materials Engineering
  - 9/2000-9/2002: Graduate Research Assistant to Dr. M. L. Wang
- Comenius University, Department of Experimental Physics
  - 9/1998-9/2000: Research Assistant to Dr. A. Jaroševič

Awards

1. Allen Rothwarf outstanding ECE graduate student award 2007, Drexel University, USA
2. IEEE Student Travel award for INTERMAG 2006 conference, San Diego, CA, USA

Peer Reviewed Publications

1. O. Hovorka, A. Berger, G. Friedman, "Estimation of exchange coupling distribution in all-ferromagnetic bilayers," *IEEE Transactions on Magnetics* **43**, 2953 (2007).
2. O. Hovorka, A. Berger, G. Friedman, "Experimental comparison of exchange bias measurement methodologies," *Journal of Applied Physics* **101**, 09E515 (2007).
3. O. Hovorka, A. Berger, G. Friedman, "Center of mass method for exchange bias measurement," *Applied Physics Letters* **89**, 142531 (2006).
4. B. B. Yellen, R. M. Erb, D. Halverson, O. Hovorka, G. Friedman "Arraying nonmagnetic colloids by magnetic nanoparticle assemblers," *IEEE Transactions on Magnetics* **42**, 3548 (2006).
5. O. Hovorka, A. Berger, G. Friedman, "Preisach model of exchange bias in antiferromagnetically coupled bilayers," *IEEE Transactions on Magnetics* **42**, 3129 (2006).
6. O. Hovorka, G. Friedman, "Energy losses in disordered hysteretic systems with dipolar interactions," *Journal of Applied Physics* **99**, 08D708 (2006).
7. O. Hovorka, G. Friedman, "Effects of interaction topology, sign and strength on hysteretic losses," *Physica B* **372**, 234 (2006).
8. B. B. Yellen, O. Hovorka, G. Friedman "Arranging matter by magnetic nanoparticle assemblers," *Proc. Natl. Acad. Sci. USA* **102**, 8860 (2005).
9. O. Hovorka, G. Friedman, "Closure of minor hysteresis loops in disordered antiferromagnetic systems," *Journal of Applied Physics* **97**, 10E514 (2005).
10. O. Hovorka, B. B. Yellen, N. Dan, G. Friedman, "Self-consistent model of field gradient driven particle aggregation in magnetic fluids," *Journal of Applied Physics* **97**, 10Q306 (2005).
11. O. Hovorka, G. Friedman, "Onset of reptations and critical hysteretic behavior in disordered systems," *Journal of Magnetism and Magnetic Materials* **290-291**, 449 (2005).
12. O. Hovorka, B. B. Yellen, G. Friedman, "Modeling stability of trapped ferromagnetic nanoparticle chains," *IEEE Transactions on Magnetics* **39**, 2549 (2003).
13. G. M. Lloyd, V. Singh, M. L. Wang, O. Hovorka, "Temperature compensation and scalability of hysteretic/anhysteretic magnetic-property sensors," *Sensors Journal IEEE* **3**, 708 (2003).